28日　B会場（小講堂）　9：00〜10：00

2

欠損を有する大腿骨に対するCT/有限要素法（第2報）

Predicting strain of the bone with a defect by a CT based finite element method

東京大学　医学部　整形外科[1]
麻布大学獣医学部第2外科[2]

○別所（べっしょ）　雅彦（まさひこ）[1]　大西五三男[1]
松本　卓也[1]　大橋　暁[1]
藤森　祥弘[2]　陰山　敏昭[2]
中村　耕三[2]

MASAHIKO BESSHO

Department of Orthopaedic Surgery, University of Tokyo

【目的】骨欠損を伴う骨の強度を非侵襲に定量評価することが可能な解析モデルを考案した。本解析法の正確性を検討するために、ビーグル大腿骨に欠損を作成し、荷重試験を行い、この結果を本法による解析結果と比較対照を行った。【方法】成犬6頭（12本）の摘出大腿骨の骨幹部に2種の欠損モデル（各群6本）を作成した。標本の定量的CTデータをもとに、海綿骨に1 mmの4節点ソリッドと皮質骨外層に0.4 mmの3節点シェルを使用し3次元解析モデルを作成した。犬骨の材料特性はヒトと同等とし（Ashman, 1984）、定量的CTデータから各メッシュに対応する骨密度を算出し、ヤング率・降伏応力をKeyakらやKellarらの方法により対応する各メッシュに割り当てた。ポアソン比は、0.4とした。荷重試験および本解析法ともに荷重・拘束条件は骨頭を解剖軸に一致して準静的に圧縮し、遠位端は拘束した。非線形解析を行い、1つの3節点シェル要素の最大主応力がその要素の臨界応力を超える場合（クラック）、または、1つの3節点シェル要素のDrucker-Prager相当応力が降伏応力を超え、かつ最小主歪みが−10000 ustarin以下の場合（圧潰）をそれぞれ骨折と定義した。骨折荷重の実験値と解析値の比較を行った。【結果】X軸を骨折荷重の解析値、Y軸を同実験値とした回帰直線は、$y=1.4046x+26.9$（$R=0.924$）であった。【考察】本法は、骨欠損を有する骨の歪みを精度よく予測でき、骨欠損を伴う強度予測を行いうる方法と考えられた。

06(XII)-90

直達式骨折整復支援装置に関する研究
-直達式骨折整復術における牽引力・整復経路測定-

○森本顕二郎[a],廖洪恩[a],杉田直彦[b],光石衛[b],中島義和[b],小山毅[d],菅野伸彦[d],
前田ゆき[e],別所雅彦[c],大橋暁[c],松本卓也[c],松山順太郎[c],岩城純一郎[f],中沢東治[f],
池田大作[g],大西五三男[c],佐久間一郎[b]
東京大学大学院{[a]新領域創成科学研究科,[b]工学系研究科,[c]医学系研究科},[d]大阪大学大学院医学系研究科,[e]大阪南医療センター,[f]THK(株),[g]瑞穂医科工業(株)

Research on the Robot for Direct Reduction of Femur
-Measurement of Direct Reduction Force and Path-

K.Morimoto[a], H.Liao[a], N.Sugita[b], M.Mitsuishi[b], Y.Nakajima[b], T.Koyama[d], N.Sugano[d], Y.Maeda[e], M.Bessho[c], A.Ohashi[c], T.Matsumoto[c], J.Matsuyama[c], J.Iwaki[f], T.Nakazawa[f], D.Ikeda[g], I.Ohnishi[c], I.Sakuma[b]
{[a]Graduate School of Frontier Sciences, [b]Graduate School of Engineering, [c]Graduate School of Medicine}, the University of Tokyo, [d]Graduate School of Medicine, Osaka University, [e]National Organization Osaka Minami Medical Center, [f]THK Co. LTD., [g]MIZUHO Ikakogyo Co .LTD.

Abstract: The patients of femoral neck fracture are increasing as the result of aging society. In fracture reduction of femur, precise positioning of bone fragment hastens patient's recovery from surgery. Surgeons have to operate accurately although fracture traction's load put excessive burdens on them. To solve the problem, we have developed a robot which can be moved accurately and function as a power assistance. In this study, measurement devices have developed to obtain the clinical data for direct fracture reduction robot. The measurement devices have 6-axix force sensor and marker for optical 3D measuring device and can measure fracture reduction force, torque and path. The measurement devices' error is enough to measure forces and torques during fracture reduction.

Key words: Fracture reduction, Femur, Force, Torque, path, Computer assisted surgery

1. 緒　言

高齢者におこりやすい骨折のなかでも大腿骨頚部骨折は寝たきりとなる可能性の高い骨折である。1997 年の調査[1]では，大腿骨頚部骨折の年間の患者数は 92,400 人であり，社会の高齢化の進行に伴い骨粗鬆症の患者が増加すると，大腿骨頚部骨折の患者も増加すると予測されている。

大腿骨頚部骨折の治療法は外科的な手術によるものがほとんどである。手術では大腿骨の遠位骨片を牽引しながら位置決めし，ピンによって遠位骨片と近位骨片を固定する。しかし，大腿筋などの周辺組織が萎縮した状態では整復のための牽引に大きな力が必要となるため術者にとって負担となる。また，X 線透視下で 2 次元の情報を用いて位置決めを行わなければならないため，術者の熟練が必要となるという問題がある。

この問題に対し，骨片の位置決めを正確に行うためのナビゲーションシステムの開発や[2]，牽引力を医師に変わって負担する骨折整復支援装置[3,4]の開発が行われている。これらが組み合わせることで，骨片の位置決めを容易にすることができると期待されている。

骨折整復支援装置[3,4]は足をブーツを介して把持し，牽引する。この牽引法は介達式と呼ばれ，患者への侵襲はないものの，足首や膝の関節の影響があるため大腿骨を動かしにくいという欠点がある。これに対して，直達式の牽引法がある。直達式では大腿骨にピンを打ち，ピンに連結されたリングを持って直接大腿骨を牽引する。骨折整復術において術後の患者の歩行機能を向上させるには，折れた骨片の精確な位置決めが重要であるが，その点では直達式のほうが優れている。

そこで我々は直達式の骨折整復支援装置の開発を行っている。しかし，装置の開発に必要である臨床における牽引力は，ほとんど報告されていない[5]。本研究では骨折整復力と骨折整復経路の臨床における使用を目指した計測器を作成した。その基礎評価を行ったので報告する。

2. 骨折整復力測定器

作成した骨折整復力測定器（Fig.1）は直達式骨折整復術に用いられるリングの任意の位置にピン固定用のクランプを介して取り付けられる。6 軸の力覚センサ(IFS-67M25A50-I40, Nitta, 定格 Fx, Fy [N]: 200; Fz [N]: 400; Mx - Mz [Nm]:13)と光学式 3 次元位置計測装置（Polaris, NDI, Canada）のマーカを有している。

最大の整復力は 30kgf を超える[5]が，このときに加わるモーメントを計測するには大きなセンサを用いる必要がある。しかし，センサ自体の重さが骨に負担となることや，患部の近くに設置することを考慮すると小型な方が望ましい。そこで，小型な 2 つのセンサを用いるこ

とで力を分散させ個々のセンサに加わるモーメントが小さくなるようにした。

3. 評価実験

直達式整復術のリングに計測器の 2 つのセンサ(センサ 1,センサ 2)と,台に固定された別のセンサ(センサ 3)を取り付け,静的な状態で力を加えた。センサによって得た値に座標変換を行うと以下の関係が成り立つ。

$${}^{p}T_{m3}\ {}^{m3}T_{s3}\ {}^{s3}F = {}^{p}T_{m1}\ {}^{m1}T_{s1}\ {}^{s1}F + {}^{p}T_{m2}\ {}^{m2}T_{s2}\ {}^{s2}F \quad (1)$$

$$\begin{aligned}{}^{p}T_{m3}\ {}^{m3}T_{s3}\ {}^{s3}M = {}&{}^{p}T_{m1}\ {}^{m1}T_{s1}\ {}^{s1}M + {}^{p}T_{m2}\ {}^{m2}T_{s2}\ {}^{s2}M \\ &+ {}^{p}V_{31} \times {}^{p}T_{m1}\ {}^{m1}T_{s1}\ {}^{s1}F \\ &+ {}^{p}V_{32} \times {}^{p}T_{m2}\ {}^{m2}T_{s2}\ {}^{s2}F \end{aligned} \quad (2)$$

p は光学式 3 次元位置計測装置,s1-s3 はセンサ 1-3,m1-m3 はセンサ 1-3 に取り付けられたマーカを意味する。${}^{\alpha}T_{\beta}$ を座標系 α による座標系 β の記述,${}^{p}V_{31}$,${}^{p}V_{32}$ を測定器の座標系によるセンサ間のベクトル,F,M を力,モーメントとした。

式(1)と式(2)における左辺と右辺の実験結果を図 2 に示す。図 2 の点線は式(1)式(2)の左辺の値であり,センサ 3 の値を位置計測装置の座標系で表した値である。また,図 2 の実線は式(1)式(2)の右辺の値であり,センサ 1 とセンサ 2 からセンサ 3 の位置での力とモーメントを計算で出し,位置計測装置の座標系で表した値である。一定の荷重を加えているときの誤差は,力で 300gf 以下,モーメントで 2000cmgf 以下であった。

この値にはセンサ自身の誤差の他,3 次元位置計測装置の誤差,リングのたわみによる誤差が含まれている。リングの把持部に加わる力の推定最大値は 30kgf 以上であるので,モータの出力や安全装置の作動力を決定するために用いる最大牽引力を推定するためには十分である。

4. 今後の予定

軟部組織と骨を模擬したモデル脚 (Sawbones) に対して,模擬整復術を行い,C-アーム X 線撮影装置で骨片の位置を確認しながら,力と位置の同時計測を行う。

滅菌についてテストした後,臨床で実際に用いる。

謝辞

本研究の一部は厚生労働科学研究費補助金(生体機能解析・補助・代替機器開発研究事業) (17100301) による。

参考文献

1) Orimo H : "Trends in the incidence of hip fracture in Japan, 1987-1997: The third nationwide survey", J Bone Miner Metab, 18: 126-131, 2000.
2) Ofer Ron, et al.: "Computer-Based Periaxial Rotation Measurement for Aligning Fractured Femur Fragments from CT: A Feasibility Study", Computer Aided Surgery, 7:332-341, 2002
3) 石堀達也,他 : "大腿骨骨折整復支援ロボットの開発",ロボティクス・メカトロニクス講演会'03 講演論文集,2P2-2F-D4,2003
4) Mamoru MITSUISHI, et al.: "Development of a Computer-Integrated Femoral Head Fracture Reduction System", Proceedings of the 2005 IEEE International Conference on Mechatronics,834-839, 2005
5) Thomas Gosing, et al.: "Force and Torque during Fracture Reduction: Intraoperative Measurements in the Femur", Journal of Orthopaedic Research, 333-338,2006

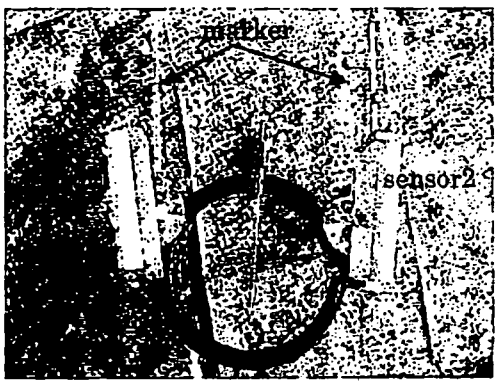

Fig.1 Measurement Devices for Fracture Reduction Force

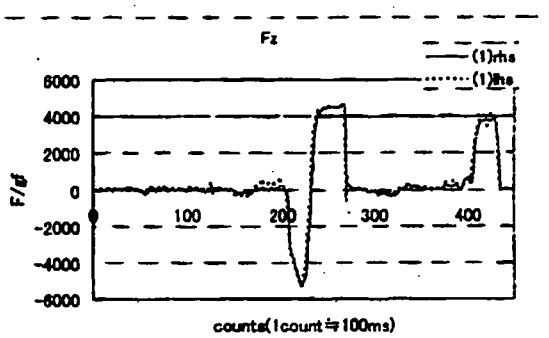

(a)

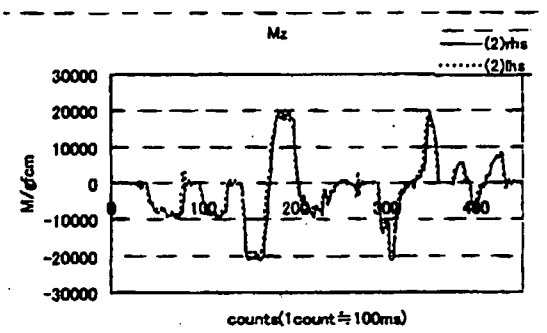

(b)

Fig2. Results of measurement devices test
(a) Reduction Force (b) Moment around reduction axis

ELSEVIER

Journal of Biomechanics 40 (2007) 1745 1753

JOURNAL OF BIOMECHANICS

www.elsevier.com/locate/jbiomech
www.JBiomech.com

Prediction of strength and strain of the proximal femur by a CT-based finite element method

Masahiko Bessho, Isao Ohnishi*, Juntaro Matsuyama, Takuya Matsumoto, Kazuhiro Imai, Kozo Nakamura

The Department of Orthopaedic Surgery, Faculty of Medicine, The University of Tokyo, 7-3-1 Hongo, Bunkyo-ku, Tokyo 113-0033, Japan

Accepted 16 August 2006

Abstract

Hip fractures are the most serious complication of osteoporosis and have been recognized as a major public health problem. In elderly persons, hip fractures occur as a result of increased fragility of the proximal femur due to osteoporosis. It is essential to precisely quantify the strength of the proximal femur in order to estimate the fracture risk and plan preventive interventions. CT-based finite element analysis could possibly achieve precise assessment of the strength of the proximal femur. The purpose of this study was to create a simulation model that could accurately predict the strength and surface strains of the proximal femur using a CT-based finite element method and to verify the accuracy of our model by load testing using fresh frozen cadaver specimens. Eleven right femora were collected. The axial CT scans of the proximal femora were obtained with a calibration phantom, from which the 3D finite element models were constructed. Materially nonlinear finite element analyses were performed. The yield and fracture loads were calculated, while the sites where elements failed and the distributions of the principal strains were determined.

The strain gauges were attached to the proximal femoral surfaces. A quasi-static compression test of each femur was conducted. The yield loads, fracture loads and principal strains of the prediction significantly correlated with those measured ($r = 0.941$, 0.979, 0.963). Finite element analysis showed that the solid elements and shell elements in undergoing compressive failure were at the same subcapital region as the experimental fracture site.

Keywords: Hip fracture; Osteoporosis; Finite element analysis; Fracture strength; Fracture site; Strain

1. Introduction

In elderly persons, hip fractures occur as a result of increased fragility of the proximal femur due to osteoporosis and have been recognized as a major public health problem. Prevention of hip fracture is a high-priority issue because of the rapid increase in the number of elderly people. It is essential to precisely quantify the strength of the proximal femur in order to estimate the fracture risk and plan preventive interventions. Clinically available methods of estimating bone strength include bone densitometry such as dual energy X-ray absorptiometry (DEXA) or peripheral quantitative computed tomography (pQCT), and imaging procedures such as X-ray or CT. These techniques evaluate regional bone density and morphology, which are partly related to fracture risk, but they are of limited value for quantifying structural strength (Faulkner et al., 1993). Therefore, it is necessary to develop a noninvasive method for accurate quantitative structural analysis that incorporates information on both morphology and bone density in a three-dimensional distribution.

CT-based finite element (FE) analysis, which incorporates information on both the three-dimensional architecture and bone density distribution, could possibly achieve precise assessment of the strength of the proximal femur (Cody et al., 1999). Previous studies on CT-based FE analysis of bone strength have shown that it accurately predicts the fracture load (Cody et al., 1999; Keyak, 2001; Keyak et al., 1998). The accuracy of previous methods has not been fully validated, because the studies only evaluated fracture loads and sites, and did not precisely assess strain

*Corresponding author. Tel.: +81 3 3815 5411; fax: +81 3 3818 4082.
E-mail address: OHNISHII-DIS@h.u-tokyo.ac.jp (I. Ohnishi).

0021-9290/$ - see front matter © 2006 Elsevier Ltd. All rights reserved.
doi:10.1016/j.jbiomech.2006.08.003

at the bone surface. Fracture occurs as a result of excessive strain and/or stress within the bone, so it represents the terminal manifestation of the loading process. However, deformation of bone during loading process should also be validated by comparison of results between analytical and experimental data. Therefore, the precision of the CT-based FE method needs to be verified by comparing the strain generated at the bone surface in an experimental setting with the calculated value.

The purpose of this study was to create a simulation model that could accurately predict the strength and surface strains of the proximal femur using a CT-based FE method. The accuracy of our model was verified with comparison of principal strains, displacement, and yield and fracture loads between the prediction and experiment by conducting load testing using fresh frozen cadaver specimens.

2. Materials and methods

Eleven right femora with no skeletal pathology were collected within 24 hours of death from 5 males aged 30 90 years (average age: 56.8 years) and 6 females aged 52 85 years (average age: 71.5 years). The cause of death was malignant lymphoma ($n = 3$), pneumonia ($n = 2$), myelodysplastic syndrome ($n = 1$), lung cancer ($n = 1$), ovarian cancer ($n = 1$), malignant fibrous histiocytoma ($n = 1$), bladder cancer ($n = 1$) and prostate cancer ($n = 1$). All of the specimens were obtained at the University of Tokyo Hospital with the approval of our ethics committee and with informed consent. Bone specimens were stored at −70 °C after each step of the protocol. Frozen specimens were trimmed with a handsaw at 140 mm distal to the midpoint of the lesser trochanter and the proximal part of each specimen was used for the experiments. After thawing, trimmed specimens were cleaned of all soft tissues (Cody et al., 1999). To prevent loss of fluid from the bone marrow, a cap of dental resin (Ostron; GC Dental Products Co., Aichi, Japan) was placed on the distal end of each specimen to seal the medullary canal. To verify the accuracy of our CT-based FE method, it was essential to precisely match the experimental conditions with those for the FE model. To identify the loading sites and constrained sites, as well as the strain gauge sites, in a FE mesh model, we matched a two-dimensional (2D) image of each specimen with the corresponding three-dimensional (3D) FE model. To perform this registration process, we utilized a fiducial-based system (Russakoff et al., 2003). We attached total of 11 circular fiducials with a radius of 2.5 mm and a width of 1.5 mm made of epoxy resin sheet (3001-01, Pacific Research Laboratories Inc., Washington, USA), comprising three for the femoral head, four for the trochanteric region, and four for the diaphysis.

The femora were immersed in water and axial CT scans were obtained with a slice thickness of 3 mm and a pixel width of 0.398 mm using Aquilion Super 4 (Toshiba Medical Systems Co., Tokyo, Japan, 120 kV, 75 mA s, 512 × 512 martix), as well as a calibration phantom (B-MAS200, Kyoto Kagaku, Kyoto, Japan) containing five hydroxy-apatite rods (0, 50, 100, 150, 200 mg/cm^3).

2.1. Quasi-static uniaxial compressive load testing

A quasi-static compression test of each femur was conducted. The proximal femur was slanted at 20° in the coronal plane (Keyak et al., 1998). A dental resin cap was molded (not bonded to the femoral head) (Keyak et al., 1998) and placed on the femoral head to apply a uniform compressive load (Fig. 1). Sliding of the cup on the loading platen was not allowed. The depth of the cap was set as 8 mm. The area of the femoral head in contact with the cap was outlined and marked using a marker pen (MO-120-MC, Zebra Co. Ltd., Tokyo, Japan). The distal diaphysis (with a length of 50 mm) was embedded in wood metal (U-ALLOY70, Osaka Asahi Metal Mfg. Co. Ltd., Osaka, Japan) (Cody et al., 1999). Eight 0°/45°/90°-stacked rosette strain gauges (KFG-1-120-D17-11L2M3S; Kyowa Electronic, Tokyo, Japan) were attached to the surface of the diaphysis and the trochanteric region of each specimen with adhesive cyano-acrylate (CC-33A; Kyowa Electronic, Tokyo, Japan), and four 0°/45°/90°-stacked rosette strain gauges (SKF-22358; Kyowa Electronic, Tokyo, Japan) were attached to the cortical surface of the femoral neck (Fig. 2). To identify the site of attachment for each strain gauge and the cap, images of the specimens were taken with a digital camera from a distance of 500 mm using a 2048 × 1536 matrix (E995; Nikon Co., Tokyo, Japan) (Fig. 3).

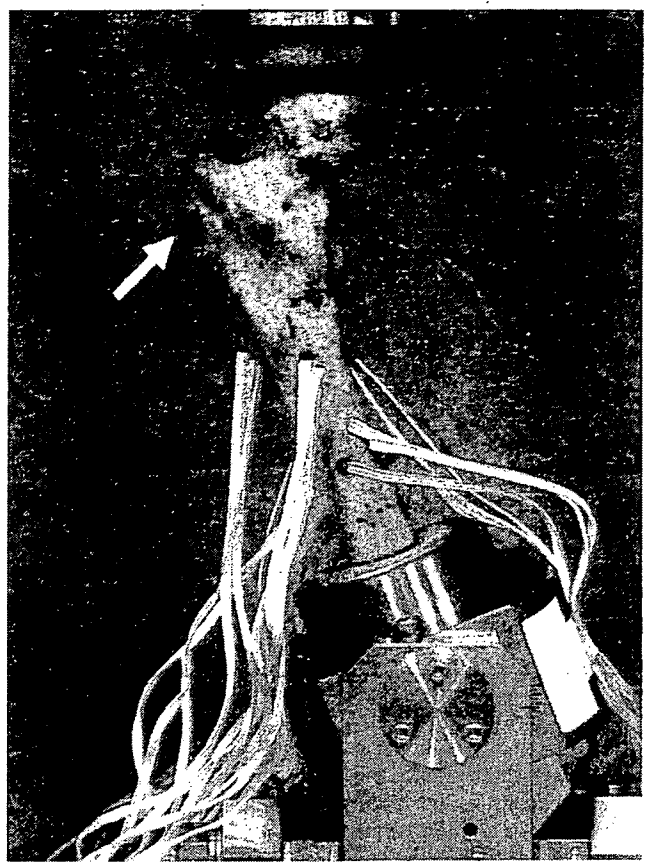

Fig. 1. Uniaxial compressive load testing. A quasi-static compression test of the femur was conducted. The proximal femur was slanted at 20° in the coronal plane and a load was applied at a rate of 0.5 mm/min after all of the fiducials (arrow) were removed.

A pre-load of about 220 N was applied (Cody et al., 1999). The specimens were compressed at a cross-head speed of 0.5 mm/min by a mechanical testing machine (Tensilon UTM-2.5T; Orientec, Tokyo) after all of the fiducials were removed (Keyak et al., 1998). The applied load was measured by using a load cell (T-CLB-5-F-SR; T. S. Engineering, Kanagawa, Japan). The magnitude of the load and the cross-head displacement were continuously recorded using MacLab/4 (AD Instruments, Castle Hill, NSW, Australia) at a sampling rate of 2 Hz. Strain at the gauge attachment sites was continuously measured and recorded throughout loading at a sampling rate of 0.5 Hz and the results were stored in a data logger (U-CAM-20PC-1; Kyowa Electronic, Tokyo, Japan). Then the maximum and minimum principal strains were calculated at each of the gauge sites.

The measured yield load was defined as the load at the point where the rate of change of the load decreased. The measured fracture load was defined as the value where the rate of change of the load per time reached zero. The loading was stopped when the rate of change of the load

declined to zero, because we did not want to induce another fracture in the specimen by applying a heavier load to accurately identify the local fracture site.

To determine the actual fracture sites, CT scans were obtained (120 kV, 150 mA s and 0.185 mm pixels), as contiguous 0.5-mm slices with a 512 × 512 matrix after mechanical testing. The CT scans were processed and reconstructed to obtain mid-coronal section images. The locations and types of the experimental fractures were judged from these reconstructed CT images.

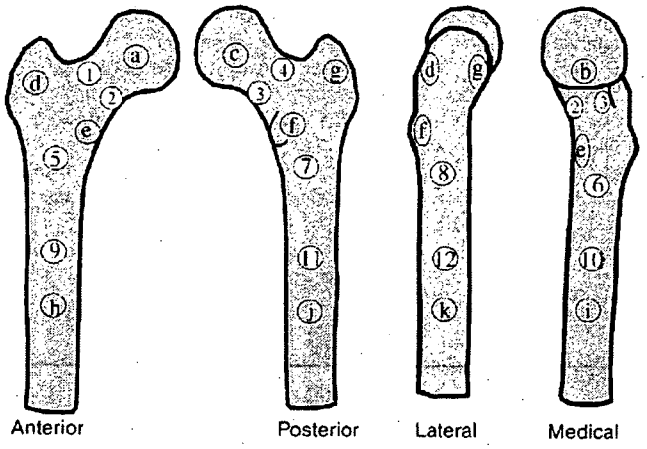

Fig. 2. Strain gauge and fiducial marker attachments. Four strain gauges (1) (4) with a gauge length of 0.6 mm were attached to the femoral neck, Eight strain gauges (5) (12) with a gauge length of 1 mm were attached to the diaphysis and the trochanteric region. A total of 11 circular fiducials were attached, including three for the femoral head (a) (c), four for the trochanteric region (d) (g), and four for the diaphysis (h) (k).

2.2. Registration

To verify the accuracy of our CT-based FE method, it was essential to precisely match the experimental conditions with the FE model. To identify the locations of the loading and constrained sites, and the sites of the strain gauges in the FE mesh model, registration of a 2D digital image and a 3D-CT image was performed by manually matching each of the four fiducials on the 2D digital image with the corresponding fiducials on the 3D-CT image using Mechanical Finder (Research Center of Computational Mechanics Inc., Tokyo, Japan). After registration, the coordinates of the strain gauge attachment sites were obtained on the 3D-CT image. By these procedures, the elements in the simulation model that corresponded with the gauge attachment sites were identified (Fig. 3). Then the mean target registration error (TRE) was calculated by the method described by Russakoff et al. (2003).

The procedure was as follows:

1. An epoxy resin plate was attached to the bone as a target instead of a strain gauge.
2. CT scanning was performed with a slice thickness of 3 mm.
3. The coordinates of the target were obtained on the 3D-CT and the target was deleted from the CT image when extraction of the bone area was performed.
4. Registration of the 2D digital image with a target and the corresponding 3D-CT image was done manually.
5. The difference between the coordinates obtained by steps 2 and 4 was calculated.
6. Steps 4 and 5 were repeated 6 times and the mean TRE was obtained.

Our preliminary investigation disclosed that the registration by matching a 2D image with a 3D-CT image under the guidance of 4 fiducials resulted in a mean TRE of 0.83 mm with a standard deviation of 0.21 mm.

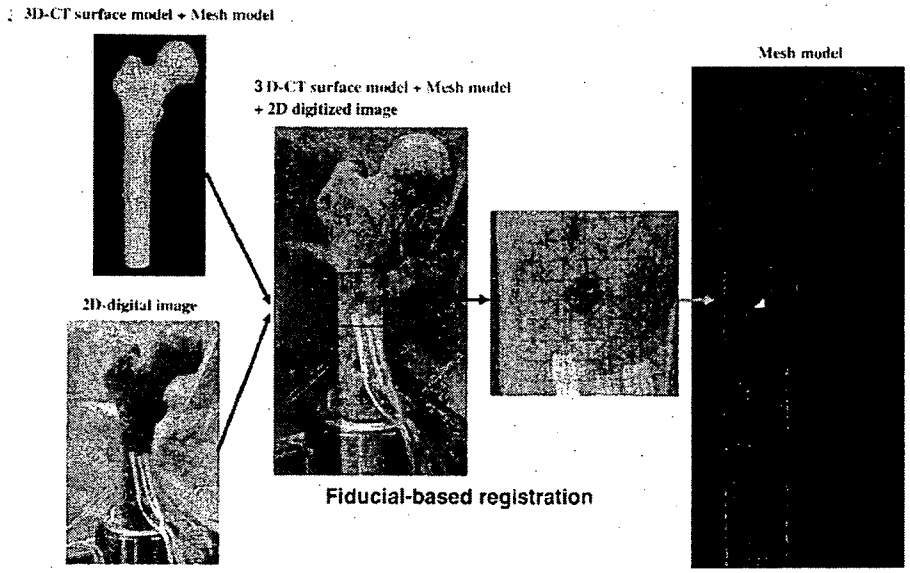

Fig. 3. Registration of the strain gauge attachment sites. Three images (a 3D-CT surface model, a mesh model, and a 2D digital image) were matched by using the fiducial markers as a guide. Registration of a 2D digital image and a 3D-CT image was performed by manually matching each of the four fiducials on the 2D digital image with the corresponding fiducials on the 3D-CT image. After registration, the coordinates of the strain gauge attachment sites were obtained on the 3D-CT image. By these procedures, the elements in the simulation model that corresponded with the gauge attachment sites were identified.

2.3. Nonlinear FE analysis

We used software that was newly developed by the authors (Mechanical Finder) to extract the bone area and for finite element analysis. The CT data were transferred to a workstation (Endeavor Pro-1000, Epson Direct Co., Nagano, Japan) and 3D FE models were constructed from the CT data. A global threshold algorithm was used to extract the bone area with a threshold of 200 mg/cm^3 (Lang et al., 1997). For extracting the bone area when the density was extremely low, we employed a closing algorithm in addition to the global threshold algorithm. The fiducial markers were excluded from the region of interest (ROI) of the 3D FE model. Because of the structural complexity of the proximal femur, we adopted tetrahedral elements instead of cubic elements to represent the smooth surface (Ulrich et al., 1998). Trabecular bone and the inner portion of cortical bone were modeled using 3 mm linear tetrahedral elements (Fig. 4). In addition, we also adopted triangular shell elements on the outer surface of cortex to accurately represent the thin cortical shell (Dalstra et al., 1995), and to reduce underestimation of the material properties of surface elements due to excessively small CT values caused by the partial volume effect. The thin shell elements were created with a thickness of 0.4 mm because the pixel width of the CT scan images (not the models) was 0.398 mm (Fig. 4). The FE mesh models were generated by the advancing front method (Ito et al., 2004). On average, there were 95,238 tetrahedral elements and 5291 triangular shell elements. The average computing time was about 10 h.

To investigate the model convergence, we created models with elements measuring 2, 3, and 4 mm, but the aspect ratio remained constant among these models. We also created a model with an element size of 1 mm, but it could not be solved due to the limited capacity of our computer. For each of the models, total strain energy was calculated at a load of 2000 N under the same loading and boundary conditions. Data on the total strain energy were compared among the models with an element size of 2, 3, and 4 mm. The total strain energy of the simulation model was reduced by 1.7 2.0% with increase of the element size from 2 to 3 mm. With an increase from 2 to 4 mm, it decreased by 3.8 9.1%. Therefore, the 3 mm model was thought to achieve sufficiently precise prediction compared with the 2 mm model, which was the most accurate among the three models. The average computing time for the 2 mm model was more than 30 h, but it was about 10 h for the 3 mm model. Keyak and Skinner (1992) previously recommended adopting an element size of less than 3 mm. For these reasons, we adopted an element size of 3 mm.

To allow for bone heterogeneity, the mechanical properties of each element were computed from the Hounsfield unit value. Ash density was approximated as equivalent to hydroxy-apatite density which neglects the effect of fat content on the Hounsfield unit value for trabecular bone (Ito et al., 1997; Keyak et al., 2005a, b). The ash density of each voxel was determined from the linear regression equation derived by relating the Hounsfield unit of a calibration phantom to its equivalent ash density. The bone density of an element was determined from the average number of Hounsfield units obtained for a total of 17 points in the element (Fig. 5). Young's modulus and the yield stress of each tetrahedral element were calculated using the equations proposed by Keyak (Keyak et al., 1998) and Keller (Keller, 1994) (Table 1). Poisson's ratio of each element was set as 0.4 (Keyak et al., 1998). In previous studies, the Young's modulus of the cortex has been found to range from 11 to 24 GPa (Bayraktar et al., 2004) or from 9 to 21 GPa (McCalden et al., 1993). Young's modulus of each triangular shell element was set as equivalent to that of the adjacent tetrahedral element located underneath the shell element and the minimum Young's modulus of the shell element was set as 10 GPa.

Nonlinear FE analysis was performed by the Newton Raphson method. To allow for the nonlinear phase, the mechanical properties of the elements were assumed to be bi-linear elastoplastic, and the post-yield modulus was set as 5% of E (where E is the pre-yield Young's modulus) (Bayraktar et al., 2004; Reilly and Burstein, 1975). According to the previous study, the ultimate strain value for trabecular bone loaded in compression ranged from −3000 to −27,900 microstrain (with an average of −11,000 microstrain) (Rohl et al., 1991), while it was −9700 to −15,600 microstrain (with an average of −11,800 microstrain) for cortical bone (Kaneko et al., 2003). Failure of a yield element in compression was

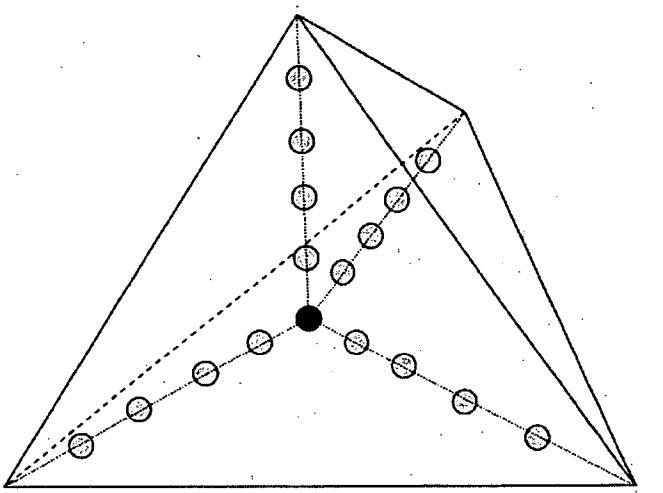

Fig. 5. Determination of bone density in tetrahedral elements. The bone density of an element was determined from the average number of Hounsfield units obtained for a total of 17 points that were composed of the center point (solid circle) and 4 points (open circles) evenly distributed on 4 lines connecting the center point to each of the apexes of the tetrahedral element.

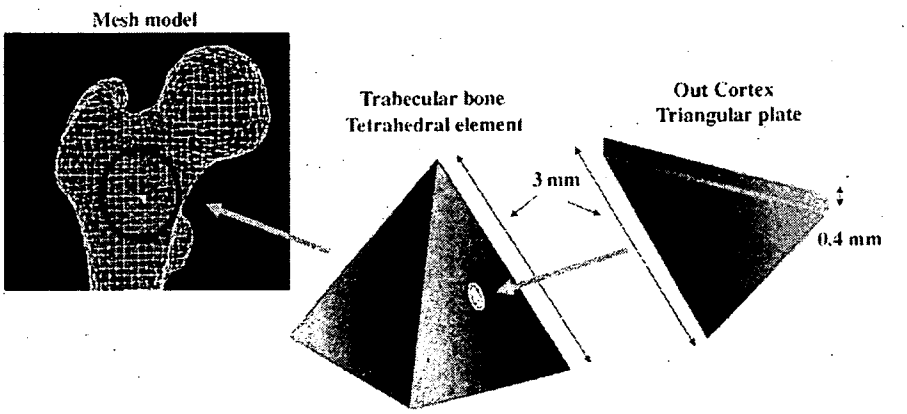

Fig. 4. Elements. Trabecular bone and the inner portion of cortical bone were modeled using 3 mm linear tetrahedral elements, while the outer cortex was modeled using 3 mm triangular plates with a thickness of 0.4 mm.

Table 1
The equations used to compute the material properties from the ash density

Ash density (g/cm^3)	Young's modulus (MPa)
$\rho = 0$	0.001
$0 < \rho \leqslant 0.27$	$33{,}900\rho^{2.20}$
$0.27 < \rho \leqslant 0.6$	$5307\rho + 469$
$0.6 < \rho$	$10{,}200\rho^{2.01}$
	Yield stress (MPa)
$\rho < 0.317$	$137\rho^{1.88}$
$0.317 \leqslant \rho$	$114\rho^{1.72}$

defined as occurring when the minimum principal strain of an element was more negative than −10,000 microstrain.

In previous studies, mechanical properties were assumed to be isotropic and to behave the same in compression and tension. We also adopted isotropic mechanical properties but the criteria for element failure differed between compressive and tensile failure (Kaneko et al., 2003; Keaveny et al., 1994). Thus, the asymmetric strength characteristics of the material were introduced into our nonlinear FE method. Previous experimental studies on the mechanical properties of bone have shown that the ultimate tensile stress of trabecular bone is only 0.79 of the compressive yield stress (Keaveny et al., 1994), while the ultimate tensile stress of cortical bone is only 0.76 of compressive yield stress (Kaneko et al., 2003). Based on these results, the ultimate tensile stress was assumed to be 0.8 times the compressive yield stress in our model.

Failure and yield of an element was judged as follows:

(1) We assessed whether the Drucker Prager equivalent stress had exceeded the element yield stress (see Appendix A). If not, the process went to (2). If yes, it went to (5).
(2) We assessed whether the maximum principal stress exceeded the element ultimate tensile stress, which was 80% of the element compressive yield stress. If yes, the element was assumed to crack in the direction of the maximum principal stress and we proceeded to (3). If not, it was judged that the element was still undergoing elastic deformation and showed no change.
(3) Young's modulus for the cracked element was set as zero in the plane of cracking. After cracking occurred in three planes, we proceeded to (4). If cracking was limited to one or two planes, the element was judged to have shown incomplete failure and still had non-zero Young's modulus in one or two planes.
(4) An element with cracking in three planes was judged to have undergone complete failure and the stress on that element was reduced to zero.
(5) After an element underwent compressive yield, Young's modulus was reduced to the post yield modulus. For each element that yielded, it was judged whether the negative value of the minimum principal strain exceeded −10,000 microstrain.

If yes, the process proceeded to (6). If not, it was judged that the element was still yielding.

(6) The element was judged to have undergone compressive failure and its stress was set at zero.

Even when the stiffness of an element was lost, calculation could continue if the surrounding elements were preserved. When a model was split into two pieces due to failure of multiple elements, calculation was stopped.

The linearity of the load displacement curve was lost after yielding of one solid element occurred. Therefore, yield of the model was defined as the point where at least one solid element yielded. Clinical fracture of large long bones becomes evident when the outer cortical shell fails. When a large long bone is placed under a load, failure of a small portion of the trabecular bone does not necessarily lead to clinical fracture if the cortical shell remains intact (Dickson et al., 2002). Therefore, fracture of the model was defined as occurring when at least one shell element failed.

Boundary conditions were applied to the FE models to represent the conditions of mechanical testing by performing 2 3D image registration. In each model, the location of the applied force was extrapolated from the registration coordinates of the resin cap base attached to the femoral head. The yield and fracture loads were calculated, while the sites where elements failed and the distributions of the maximum and minimum principal strains were determined. The principal strains at 50% of the experimental yield load were calculated, and all elements were in the elastic phase at this load. In each specimen, the predicted yield load was smaller than the experimental value. The predicted fracture load was also smaller than the experimental value. Therefore, comparison of post-yield strain between simulated and experimental data was performed at a load which caused both simulated and experimental yield. Likewise, comparison of post fracture strain was done at the experimental load causing fracture. The load displacement curve from the model was plotted on the corresponding experimental load displacement curve.

Pearson's correlation analysis and analysis of covariance were used to evaluate correlations between the predicted and measured values of the yield load, the fracture load, and the principal strains (Altman and Gardner, 1988). Statistical data were considered significant when p-values were less than 0.05.

3. Results

There was a significant linear correlation between the yield load predicted by FE analysis and the measured values ($r = 0.941$, 95% confidence interval, 0.786–0.985; standard error of the estimate SEE = 394 N; $p < 0.0001$) (Fig. 6). A significant linear correlation was also noted between the predicted fracture load and the measured values ($r = 0.979$, 95% confidence interval, 0.920–0.995;

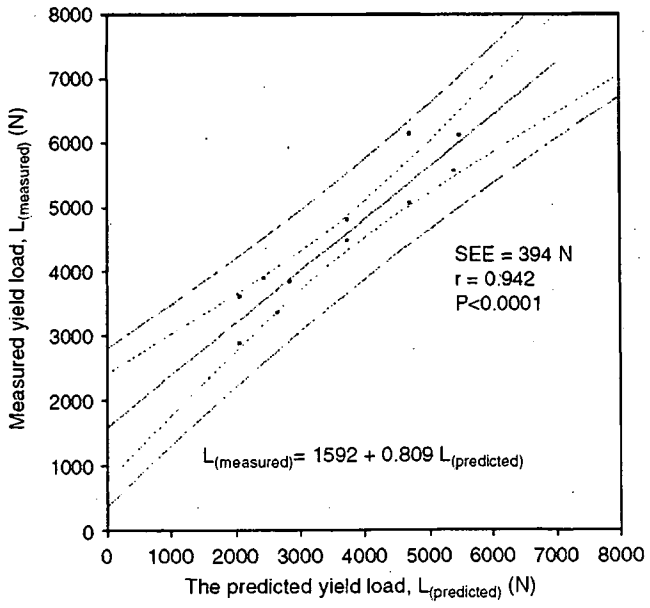

Fig. 6. Correlation between the measured and predicted yield loads. 95% confidence intervals for the regression (short dashes) and population (long dashes) are shown.

SEE = 228 N; $p<0.0001$). The slope was 0.936 (not significantly different from 1, $p = 0.75$) with an intercept of 641 N (not significantly different from 0, $p = 0.08$) (Fig. 7).

The result of comparison between the predicted and measured strains was shown in Table 2. Each slope of the regression lines for the relation between predicted principal strains in the elastic, plastic, and post-failure region and the experimental values was significantly different from 1 ($p<0.001$, <0.001, $=0.001$), while each intercept was not significantly different from 0 ($p = 0.23$, $= 0.10$, $= 0.93$). Statistically, no significant difference among the slopes of the three regression lines was recognized (at the elastic, plastic and post-failure region) ($p = 0.88$).

Typical FE and actual load–displacement curves from the specimen FR07 were illustrated (Fig. 8).

The reconstructed CT images revealed the locations of the experimental fractures. In all specimens, it was noted that the trabeculae in the subcapital region collapsed under the load applied. FE analysis showed that the solid elements and shell elements in undergoing compressive failure were at the same subcapital region as the experimental fracture site. This also contributed to confirming the accuracy of the simulation model. In addition, FE analysis of the minimum principal strain on the mid-coronal section disclosed that the area with a large negative value of the predicted minimum principal strain agreed well with the experimental fracture site (Figs. 9 and 10).

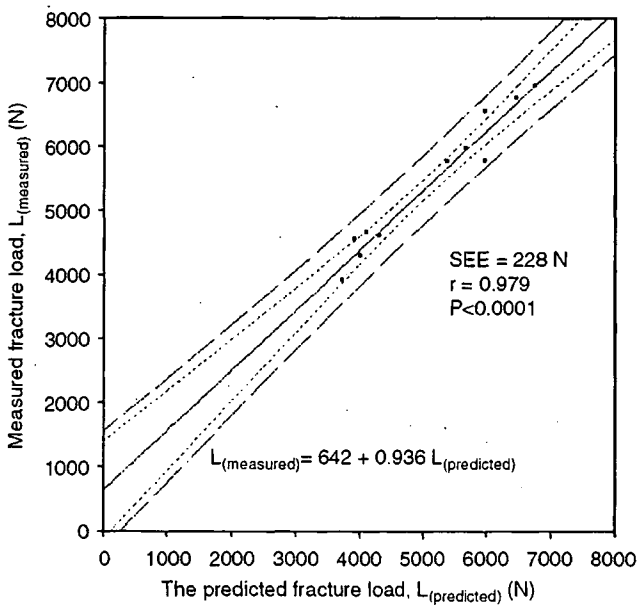

Fig. 7. Correlation between the measured and predicted fracture loads. 95% confidence intervals for the regression (short dashes) and population (long dashes) are shown.

4. Discussion

The purpose of our study was to create a clinically useful method of predicting the strength of the proximal femur noninvasively in patients with a high fracture risk. We would like to produce a precise model that can predict strength, strain and sites at fracture risk of the proximal femur more accurately than the previous models.

Keyak reported that the slope and the intercept of the regression line for the relation between predicted and experimental fracture loads was 0.77 and 1150 N (SEE: 870 N, $r = 0.962$), respectively (Keyak, 2001). On the other hand, Cody et al. (1999) reported that the correlation coefficient for the relation between predicted stiffness and experimental fracture load was 0.91. The coefficient obtained in our study was not inferior to that obtained in previous studies. The standard error of the estimate was 228 N and it was smaller than previously reported. In Keyak's study from 2001, the slope of the regression line was different from 1 but it did not deviate from 1 in our model.

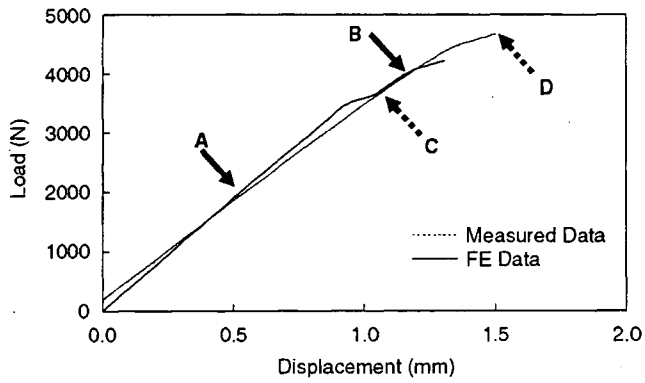

Fig. 8. Typical FE and actual load displacement curves (FR07). Dash line: FE load displacement curve. Solid line: Actual load displacement curve. Point A indicates the yielding of one or more solid elements. Point B indicates the failure of one or more shell elements. Point C indicates the occurrence of experimental yielding. Point D indicates the occurrence of experimental fracture as defined by our criterion.

Table 2
Linear regression equations for measured principal strains ($Strain_{(measured)}$ microstrain) versus FE-predicted principal strains ($Strain_{(predicted)}$ microstrain)

Phase	Regression equation	r	95% Confidence interval of r	p	$SEE_{(micro\ strain)}$
Elastic phase	$Strain_{(measured)} = -16.7 + 0.912\ Strain_{(analysis)}$	0.963	$0.954<r<0.971$	<0.0001	223
Plastic phase	$Strain_{(measured)} = -47.1 + 0.919\ Strain_{(analysis)}$	0.964	$0.955<r<0.972$	<0.0001	460
Post-failure phase	$Strain_{(measured)} = -4.22 + 0.927\ Strain_{(analysis)}$	0.950	$0.934<r<0.962$	<0.0001	693

In previous studies, Von Mises equivalent stress has been adopted as the criterion for yielding of elements (Keyak et al., 1998; Lotz et al., 1991). Although such a criterion may be suitable for ductile materials such as metal, bone is classified as one of the brittle materials. Generally speaking, the ultimate strain of metals that reaches failure is dozens of times larger than that of the bone. Therefore, bone is thought to be brittle rather than ductile. The tensile strength of bone is smaller than its compressive strength, which suggests that bone should be treated as one of the brittle materials (Cordey and Gautier, 1999). Therefore, we adopted the Drucker–Prager equivalent stress, which takes the contribution of hydrostatic stress into consideration, as the yield criterion. When hydrostatic stress is present, J_1 becomes negative, so $F(\sigma)$ becomes smaller under such condition (see Appendix A). An element has to be subjected to a larger external load for its Drucker–Prager equivalent stress to be sufficiently large to fit the yield criterion. Thus, by introducing the Drucker–Prager equivalent stress as the yield criterion, a larger external load is necessary to cause the yielding of an element.

Fig. 9. Fracture sites in a tested specimen (FR02). The arrows indicate the fracture site. The specimen sustained a fracture of the subcapital region.

Keyak et al. (1993) compared the strain in the elastic region predicted by simulation with the experimental data. The correlation coefficient for the relation between predicted and experimental strain values reported by Keyak was 0.769, with 20 data points and a confidence interval of 0.543–0.904. The correlation was inferior to ours. One of the reasons for this would be that they used cube-shaped elements, so the surface of the model became uneven and accurate matching between the gauge attachment sites and the corresponding elements in the model was technically difficult. The correlation coefficient for the relation between the predicted stress and the stress converted from the measured strain that was reported by Lengsfeld et al. was 0.91–0.94. They assumed that the cortical bone modulus was 15 GPa and surface stress values were also calculated on this basis. Because their data set had 495 items, the confidence interval was calculated to be 0.893–0.924 ($r = 0.91$) or 0.928–0.949 ($r = 0.94$). They created two kinds of models with elements having a different shape (geometry-based eight-node isoparametric brick elements and hexahedral voxel-based elements). They adopted a homogeneous Young's modulus of 1.1 GPa for trabecular bone, 20 MPa for intramedullary tissue, and 15 GPa for cortical bone (Lengsfeld et al., 1998). These homogeneous properties were thought to be one of the reasons that their correlation was inferior to ours. Ota et al. (1999) also reported a correlation coefficient of 0.81 for the relation between the predicted and experimental strains. Because their data set had 18 items, the confidence interval was calculated to be 0.552–0.926, which is inferior to ours. They did not use shell elements for outer cortex and their method matching the strain gauge sites with the corresponding model elements was not clearly described. The accuracy of models was also investigated using surface stress measurement by Dalstra et al. (1995). Young's modulus of the cortical bone was assumed to be 17 GPa and measured strain values were converted to stresses. They reported that better agreement was obtained between the predicted stress and the stress converted from the measured strain by a model with heterogeneous mechanical

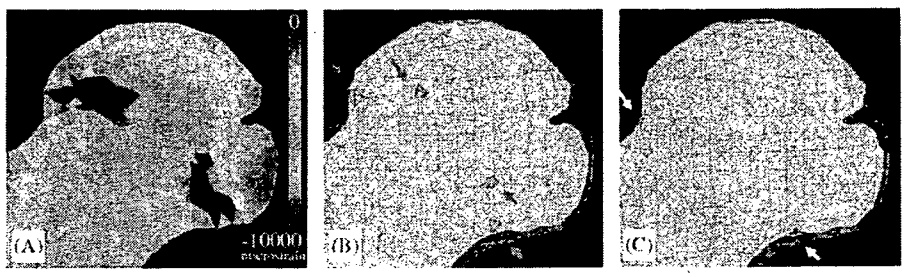

Fig. 10. Predicted fracture sites. (A) The minimum principal strain distribution under the predicted fracture load is shown for a mid-sagittal section by the FE model. The area with the lowest minimum principal strain is at the subcapital region. (L; lateral, M; Medial). (B) The failed tetrahedral elements in the mid-sagittal section (arrows) predicted by FE analysis. (C) The failed triangular elements in the mid-sagittal section (arrows) predicted by FE analysis.

properties than by a model with homogeneous properties, but they did not report the details of their statistical analysis.

We identified the actual fractures in the specimens by using reconstructed CT images of the tested specimens. In a preliminary study, we took soft X-ray films of the specimens, but it was impossible to detect the fractures. On the reconstructed CT images, fracture of both the trabecular and cortical bone was clearly seen at the subcapital region of the femoral neck, as shown by a defect or discontinuity of the bone. With the loading conditions adopted for our experiment, the compressive load caused invagination of the subcapital region of the femoral neck into the base of the femoral head. The trabecular and cortical bone of the subcapital region were crushed by the compressive load and a gap was created after the load was removed from the specimens. Clinically, this type of fracture was considered to resemble a Garden type I fracture (Garden, 1961). Stepwise analysis of the model disclosed that with an incremental increase of the load, the tetrahedral elements yielded and failure of the triangular plate elements finally occurred. The process of fracture in our model was also thought to be fairly realistic from the results of the experiment.

Few studies have compared the predicted fracture site with that obtained experimentally and have clearly shown agreement between them. Keyak et al. (2001) compared the experimental fracture site on radiographs with that shown by the 15 contiguous failure elements in their simulation model. A linear finite element method was utilized. They reported that the predicted fracture sites agreed well with the experimental sites for 13 out of 18 specimens with the stance configuration. However, evaluation of the actual correspondence of the fracture site is thought to be difficult because the area occupied by the 15 contiguous elements was quite large compared with that of the experimental fractures. Ota et al. (1999) also reported on the accuracy of fracture site prediction, but they only presented the findings for one case. In the report by Keyak (2001), she adopted a non-linear method and prediction of the fracture site was precise in 15 out of 18 cases. She reported that the predicted fracture site was located in the sub-capital region in all specimens. This was similar to our findings. We confirmed the experimental fracture sites in detail on reconstructed CT scans of the specimens that had undergone mechanical testing. Agreement of the experimental fracture sites with the locations of the failure elements and the areas with large negative values of the minimum principal strain in the models was accurately verified by matching the reconstructed CT images with those of the models.

We used a bi-linear elastoplastic model for cortical and trabecular bone under compression. In our model, the same post-yield modulus was used for both cortical and trabecular bone because of the limitation that an independent value could not be set for each of cortical and trabecular bone.

The same criterion was used for the yield of both cortical and trabecular bone. Our method determined the mechanical properties of bone from the density, and therefore had the limitation that cortical bone could not be completely distinguished from trabecular bone. A common ultimate strain value was necessary as a criterion for the compressive yield of both cortical and trabecular bone.

The advantage of a CT-based FE method is that it allows three-dimensional structural analyses, such as quantification of the bone strain and fracture load, as well as determination of the sites with a high fracture risk in the 3D simulation model. This method can supply patient-specific data that precisely assess the fracture risk for each patient. However, image quality may deteriorate in vivo due to the influence of pelvis or soft tissues. Keyak et al. have compared the accuracy of predicting bone strength between the in vitro and in situ situations, and they reported that the in situ results were overestimated by 5–13% (Keyak and Falkinstein, 2003), which could be another limitation for applying this method clinically. So we need to further investigate the accuracy of predicting strength using cadaveric specimens in situ.

Acknowledgements

This work was funded by a grant in aid for Scientific Research received from the Japan Society for the Promotion of Science (14657356).

Appendix A. The Drucker–Prager yield criterion

The Drucker–Prager yield criterion was presented by Drucker and Prager (1952) as an approximation to the Mohr–Coulomb law and a modification of the Von Mises yield criterion (Owen and Hinton, 1980).

Drucker–Prager yield criterion is described by the following equations, i.e. the influence of a hydrostatic stress component on yielding was introduced by inclusion of an additional term in the Von Mises expression

$$F(\sigma) = aJ_1 + (J_2')^{1/2}, \tag{1}$$

$$J_1 = \sigma_x + \sigma_y + \sigma_z, \tag{2}$$

$$J_2' = \tfrac{1}{2}\left(\sigma_x'^2 + \sigma_y'^2 + \sigma_z'^2\right) + \tau_{xy}^2 + \tau_{yz}^2 + \tau_{xz}^2, \tag{3}$$

where $F(\sigma)$ is a yield function, σ is the stress tensor, σ_x, σ_y and σ_z are the normal stress, τ_{xy}, τ_{yz} and τ_{xz} are the shear stress, the prime ($'$) is used to indicate the deviatoric stress, J_1 is the first stress invariant and J_2' is the second deviatoric stress invariant. α is a parameter that reflects the dilative potential of the material and it is related to the proportions of the volumetric and deviatoric strains. α is set as 0.07 (Kupfer and Gerstle, 1973)

$$\left[\text{Deviatoric stress } \sigma_{ij}' = \sigma_{ij} - \delta_{ij}\sigma_m, \quad \sigma_m = \tfrac{1}{3}\sigma_{ii}\right].$$

References

Altman, D.G., Gardner, M.J., 1988. Calculating confidence intervals for regression and correlation. British Medical Journal (Clinical Research Edition) 296, 1238 1242.

Bayraktar, H.H., Morgan, E.F., Niebur, G.L., Morris, G.E., Wong, E.K., Keaveny, T.M., 2004. Comparison of the elastic and yield properties of human femoral trabecular and cortical bone tissue. Journal of Biomechanics 37, 27 35.

Cody, D.D., Gross, G.J., Hou, F.J., Spencer, H.J., Goldstein, S.A., Fyhrie, D.P., 1999. Femoral strength is better predicted by finite element models than QCT and DXA. Journal of Biomechanics 32, 1013 1020.

Cordey, J., Gautier, E., 1999. Strain gauges used in the mechanical testing of bones. Part I: theoretical and technical aspects. Injury 30 (Suppl. 1), A7 A13.

Dalstra, M., Huiskes, R., van Erning, L., 1995. Development and validation of a three-dimensional finite element model of the pelvic bone. Journal of Biomechanical Engineering 117, 272 278.

Dickson, K.F., Galland, M.W., Barrack, R.L., Neitzschman, H.R., Harris, M.B., Myers, L., Vrahas, M.S., 2002. Magnetic resonance imaging of the knee after ipsilateral femur fracture. Journal of Orthopaedic Trauma 16, 567 571.

Drucker, D.C., Prager, W., 1952. Soil mechanics and plastic analysis of limit design. Quarterly of Applied Mathematics 10, 157 165.

Faulkner, K.G., Cummings, S.R., Black, D., Palermo, L., Gluer, C.C., Genant, H.K., 1993. Simple measurement of femoral geometry predicts hip fracture: the study of osteoporotic fractures. Journal of Bone and Mineral Research 8, 1211 1217.

Garden, R.S., 1961. Low-angle fixation in fractures of the femoral neck. The Journal of Bone and Joint Surgery 43-B, 647 663.

Ito, M., Lang, T.F., Jergas, M., Ohki, M., Takada, M., Nakamura, T., Hayashi, K., Genant, H.K., 1997. Spinal trabecular bone loss and fracture in American and Japanese women. Calcified Tissue International 61, 123 128.

Ito, Y., Shih, A.M., Soni, B.K., 2004. Reliable isotropic tetrahedral mesh generation based on an advancing front method. In: Proceedings of the 13th International Meshing Roundtable. Sandia National Laboratories, Williamsburg, VA.

Kaneko, T.S., Pejcic, M.R., Tehranzadeh, J., Keyak, J.H., 2003. Relationships between material properties and CT scan data of cortical bone with and without metastatic lesions. Medical Engineering and Physics 25, 445 454.

Keaveny, T.M., Wachtel, E.F., Ford, C.M., Hayes, W.C., 1994. Differences between the tensile and compressive strengths of bovine tibial trabecular bone depend on modulus. Journal of Biomechanics 27, 1137 1146.

Keller, T.S., 1994. Predicting the compressive mechanical behavior of bone. Journal of Biomechanics 27, 1159 1168.

Keyak, J.H., 2001. Improved prediction of proximal femoral fracture load using nonlinear finite element models. Medical Engineering and Physics 23, 165 173.

Keyak, J.H., Falkinstein, Y., 2003. Comparison of in situ and in vitro CT scan-based finite element model predictions of proximal femoral fracture load. Medical Engineering and Physics 25, 781 787.

Keyak, J.H., Fourkas, M.G., Meagher, J.M., Skinner, H.B., 1993. Validation of an automated method of three-dimensional finite element modelling of bone. Journal of Biomedical Engineering 15, 505 509.

Keyak, J.H., Rossi, S.A., Jones, K.A., Skinner, H.B., 1998. Prediction of femoral fracture load using automated finite element modeling. Journal of Biomechanics 31, 125 133.

Keyak, J.H., Rossi, S.A., Jones, K.A., Les, C.M., Skinner, H.B., 2001. Prediction of fracture location in the proximal femur using finite element models. Medical Engineering and Physics 23, 657 664.

Keyak, J.H., Kaneko, T.S., Rossi, S.A., Pejcic, M.R., Tehranzadeh, J., Skinner, H.B., 2005a. Predicting the strength of femoral shafts with and without metastatic lesions. Clinical Orthopaedics and Related Research 439, 161 170.

Keyak, J.H., Kaneko, T.S., Tehranzadeh, J., Skinner, H.B., 2005b. Predicting proximal femoral strength using structural engineering models. Clinical Orthopaedics and Related Research, 219 228.

Keyak, J.H., Skinner, H.B., 1992. Three-dimensional finite element modelling of bone: effects of element size. Journal of Biomedical Engineering 14, 483 489.

Kupfer, H.B., Gerstle, K.H., 1973. Behavior of concrete under biaxial stresses. Journal of Engeering Mechanics Division, ASCE 99, 853 866.

Lang, T.F., Keyak, J.H., Heitz, M.W., Augat, P., Lu, Y., Mathur, A., Genant, H.K., 1997. Volumetric quantitative computed tomography of the proximal femur: precision and relation to bone strength. Bone 21, 101 108.

Lengsfeld, M., Schmitt, J., Alter, P., Kaminsky, J., Leppek, R., 1998. Comparison of geometry-based and CT voxel-based finite element modelling and experimental validation. Medical Engineering and Physics 20, 515 522.

Lotz, J.C., Cheal, E.J., Hayes, W.C., 1991. Fracture prediction for the proximal femur using finite element models: Part I—linear analysis. Journal of Biomechanical Engineering 113, 353 360.

McCalden, R.W., McGeough, J.A., Barker, M.B., Court-Brown, C.M., 1993. Age-related changes in the tensile properties of cortical bone. The relative importance of changes in porosity, mineralization, and microstructure. The Journal of Bone and Joint Surgery 75-A, 1193 1205.

Ota, T., Yamamoto, I., Morita, R., 1999. Fracture simulation of the femoral bone using the finite-element method: how a fracture initiates and proceeds. Journal of Bone and Mineral Metabolism 17, 108 112.

Owen, D.R.J., Hinton, E., 1980. Finite elements in plasticity: theory and practice. In: Owen, D.R.J. (Ed.), Elasto-plastic Problems in Two Dimensions. Pineridge Press Limited, Swansea, UK, pp. 215 231.

Reilly, D.T., Burstein, A.H., 1975. The elastic and ultimate properties of compact bone tissue. Journal of Biomechanics 8, 393 405.

Rohl, L., Larsen, E., Linde, F., Odgaard, A., Jorgensen, J., 1991. Tensile and compressive properties of cancellous bone. Journal of Biomechanics 24, 1143 1149.

Russakoff, D.B., Rohlfing, T., Shahidi, R., Kim, D.H., Adler, J.R., Maurer, C.R., 2003. Intensity-based 2D 3D spine image registration incorporating one fiducial marker. Medical Image Computing and Computer-Assisted Intervention 2878, 287 294.

Ulrich, D., van Rietbergen, B., Weinans, H., Ruegsegger, P., 1998. Finite element analysis of trabecular bone structure: a comparison of image-based meshing techniques. Journal of Biomechanics 31, 1187 1192.

Available online at www.sciencedirect.com
SCIENCE DIRECT
Medical Engineering & Physics 28 (2006) 588–595
Medical Engineering & Physics
www.elsevier.com/locate/medengphy

Technical note

A new method for measurement of bone deformation by echo tracking

J. Matsuyama [a], I. Ohnishi [a,*], R. Sakai [b], H. Suzuki [b], A. Harada [b], M. Bessho [a], T. Matsumoto [a], K. Nakamura [a]

[a] *Department of Orthopaedic Surgery, University of Tokyo, 7-3-1 Hongo, Bunkyo-ku Tokyo 113-0033, Japan*
[b] *Research Laboratory, Aloka Co. Ltd., Tokyo, Japan*

Received 18 February 2005; received in revised form 14 August 2005; accepted 27 September 2005

Abstract

No method has been available to noninvasively detect bone deformation or strain under loading in vivo. We focused on ultrasonic measurement of the displacement at a certain point on a bone using the echo-tracking method (ET). To develop a method that can noninvasively detect bone deformation in vivo, a preliminary investigation was performed.

We investigated the accuracy of measuring displacement with our echo tracking system by using a flat metal panel and found that the method could measure displacement with a precision of a few microns.

A three-point bending test of a porcine tibia with both ends fully constrained was performed to measure bone surface displacement, and simultaneous measurement of the surface strain was done using two strain gauges. The correlation between the displacement measured by ET and the strain gauge readings was completely linear ($r=0.999$), showing that the method could precisely detect bone deformation. The loads versus displacement curves obtained with cyclic loading were typical hysteresis loops that showed viscoelastic properties of the measured bone.

We also improved a multi-ET system capable of simultaneously tracking multiple points to detect deformation of the bone surface. Measurement by this echo tracking system was also compared with strain gauge readings during a three point bending test with both ends of the tibia supported. The linearity of both methods was very high ($r=0.998$). Our ET method might have considerable potential for noninvasive measurement of bone viscoelasticity and plasticity.

Keywords: Echo tracking; Bone deformation; Noninvasive measurement; Bone strain

1. Introduction

Bone is a self-repairing structural material that adapts its mass, shape, and properties to changes in mechanical requirements and tolerates voluntary physical activity throughout life without breaking or causing pain. Quantifying the mechanical inputs into bone is important for understanding the form and function of the skeleton. The forces applied to each bone at the organ level must be translated to the cellular level and then somehow play a role in the maintenance and adaptation of bone tissue [1–3].

Bone fails if subjected to a force exceeding its strength, but even physiological loading during daily activities causes deformation depending on a bone's mechanical properties. Determining the extent of which deformation normally occurs should help to elucidate the mechanotransduction mechanism in bone [4]. Therefore, it is important to be able to quantitatively measure the extent of bone deformation or strain under loading.

To date, many methods have been tried to detect bone deformation under a load [5,6]. A strain gauge is a device that measures the deformation of materials to which it is attached, and this has been the method used to quantify bone strains in vivo. The strain gauge is thus the gold standard for measuring bone deformation in vivo and this device has provided much useful data [7,8]. However, measurement with strain gauges requires invasive exposure of a site for attachment to the bone surface. To date, no method has been available to noninvasively detect bone deformation or strain under loading.

* Corresponding author. Tel.: +81 3 5800 8656; fax: +81 3 3818 4082.
E-mail address: OHNISHII-DIS@h.u-tokyo.ac.jp (I. Ohnishi).

1350-4533/$ – see front matter © 2005 IPEM. Published by Elsevier Ltd. All rights reserved.
doi:10.1016/j.medengphy.2005.09.005

A NEW METHOD FOR ACCURATE MEASUREMENT OF BONE DEFORMATION WITH ECHO TRACKING

*Matsuyama, J; +*Ohnishi, I; **Sakai, R; **Suzuki, H; **Harada, A; *Bessho, M; *Matsumoto, T; *Nakamura, K
+*Department of Orthopaedic Surgery University of Tokyo, Tokyo, Japan **Research Laboratory, Aloka Co., Ltd., Tokyo, Japan
email: ohnishii- dis@ h.u-tokyo.ac.jp

Introduction

It is clinically significant to quantitatively measure degree of deformation or strain of bone under a certain load; however no method has been available to non-invasively detect bone deformation or strain under loading. Ultrasonic wave can penetrate soft tissues and visualize bone surface. Utilizing an echo-tracking (ET) method, it is possible to accurately and dynamically detect displacement of a certain point on the bone surface. The ET method is a technique measuring minute displacement of a certain point on a tissue with superior accuracy to standard ultrasound by detecting a wave pattern in a radiofrequency (RF) echo signal reflected from the tissue.

The final goal of this investigation is to develop a method to non-invasively detect bone deformation under a load in vivo using an ultrasound ET method, and for this purpose, a preliminary investigation was performed to make sure that our method had sufficient accuracy to detect bone surface deformation by conducting an in vitro experiment.

Materials and Methods

We developed an ET system to accurately measure the displacement on the surface of a bone. The accuracy of the ET system was evaluated by using a flat metal panel. The displacement of the panel was measured simultaneously by an ET system and a linear potentiometer (AT-104: Keyence Corporation, Osaka, Japan) and the standard deviation (SD) of the difference was calculated.

To evaluate how accurately the ET system can detect bone deformation under loading by monitoring displacement of the point on the bone surface, a three point bending (TPB) test of a porcine tibia was performed to measure displacement of the surface of the tibia with the ET system. After removing soft tissues, the tibia was placed with its medial aspect upwards on the testing machine (Tensilon UTM-2.5T: A&D Co., Ltd., Tokyo, Japan) and both ends of the tibia were fully restrained with dental resin (GC Ostron2®: GC, Tokyo, Japan) with a span of 214 mm. Two strain gauges (KGF-1: Kyowa Electronic Instruments, Tokyo, Japan) were attached on the posterior aspect of the tibia at 50 mm proximal and 50 mm distal from the center of the tibia, respectively. Displacement of the osseous surface was measured with a 7.5MHz linear electronic echo probe (UST-5710-7.5: Aloka, Tokyo, Japan) throughout the loading process. The maximum principal strain at each of the gauge sites was calculated from the strain gauge reading. The probe was fixed, so that the direction of the echo beam was parallel to that of loading. A single cycle load and a 3cycle load of 5780 N were applied with an actuator speed of 0.1 mm/sec for a distance of 0.7 mm. The maximum principal strain measured by the two strain gauges was compared with the displacement shown by the ET system.

We also devised the ET system capable of tracking multiple points. Five tracking points were set along the long axis of the probe with each span of 10 mm. Each displacement of the five points was simultaneously measured, and the surface deformation was shown by a third order spline complement curve which was defined by the displacements of the five points measured by the ET system. Then, the ET system strain (ETS) was defined to represent surface deformation by the following equation. ETS = D / L, where L was the distance from the first tracking point to the fifth, and D was the maximum distance from the spline curve to the straight line connecting the first tracking point and the fifth. With this multi-ET system, it was assumed that the displacement caused by translation to the direction of the echo beam and rotation in the plane including a loading point and five tracked points was cancelled.

To prove the multi-ET system could detect bone deformation even when the measured object underwent some translation, we also conducted a TPB test with both metaphyses of the porcine tibia simply supported. After removing soft tissues, the tibia with a length of 230 mm was placed horizontally on the testing machine (Servo Pulser, Shimadzu Corporation, Tokyo, Japan) with its medial aspect upwards and both metaphyses were supported by rollers with a span of 115 mm. Deformation was measured simultaneously with a 7.5 MHz linear probe and strain on the posterior surface of the tibia was measured with the strain gauge (KGF-1, Kyowa, Tokyo, Japan). Five tracking points were set along the long axis of the tibia with the center point corresponding to the site of loading. The echo probe was fixed parallel to the posterior surface of the tibia. Two strain gauges were attached along the tracking line (a straight line formed by the five tracking points) at 5 mm distal and 5 mm proximal to the center point and with each gauge axis parallel to the tracking line. Incremental load increases were applied by a resin pusher from a preload of 100 N up to 1500 N. The loading rate was set at 25 N/sec. Under each load, the ETS value and the readings of the two strain gauges were determined. The correlation between the ETS value and each of the strain gauge readings was calculated with Pearson's correlation analysis.

Results

For measurement of the displacement of the flat panel, the standard deviation (SD) of the difference was ±2.6 μm.

In the TPB test with both ends of the tibia fully restrained, the strain gauge reading and ET had excellent linearity all through the loading process (r = 0.999 and 0.996, respectively) (Fig. 1-A). The curve relating the load magnitude with the data obtained from each strain gauge was a typical hysteresis loop, indicating the measured bone was a viscoelastic material. The curve for the relationship between the load magnitude and the displacement of the ET system was also a hysteresis loop (Fig. 1-B).

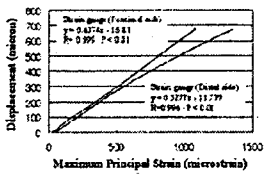

Fig. 1-A Result of the TPB test using the single-cycle load.

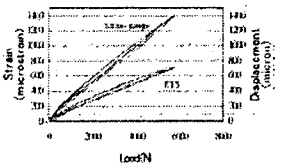

Fig. 1-B Result of the TPB test using the three-cycle load.

In the study with the multi-ET system, the strain readings of each gauge and the data from the ET system showed a perfect linear increase with the load. There was a linear relation between ET data and each of the strain gauges (r = 0.998 and 0.998, respectively) (Fig.2-A, B).

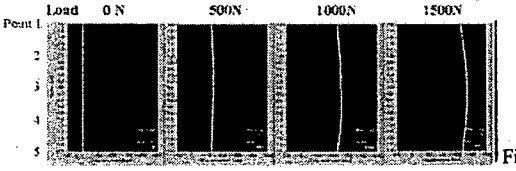

Fig. 2-A

Fig. 2-B

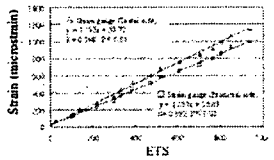

Fig. 2-A Result of the multi-ET system. The surface deformation was visualized by a third order spline complement curve.
Fig. 2-B Correlation between the strain readings of each gauge and the data from the ET system.

Discussion

In the TPB test of the fully restrained porcine tibia, the correlation between the displacement measured by ET and the strain gauge readings was very strong. Under a cyclic load, the system was able to monitor bone viscoelasticity because the load versus displacement curve was a hysteresis loop.

The magnitude of the strain measured by the strain gauges was an average strain of 1mm gauge length, while the multi ET system measured an average strain of 40 mm. However, as shown by the results of the TPB test with both metaphyses supported, linearity of both measurements was very strong, which indicated the possibility of using the ET method to detect bone surface strain even when the measured object underwent some translation.

Our ET system had sufficient accuracy to detect bone surface deformation in vitro. Further investigation is necessary to apply this method for in vivo measurement.

52nd Annual Meeting of the Orthopaedic Research Society
Paper No: 1776

To overcome the above-mentioned limitations in the measurement of bone deformation, we focused on the use of ultrasound because of its noninvasiveness. Ultrasonic waves can penetrate soft tissues and visualize the bone surface. In addition, precise measurement of the displacement of a specific point can be achieved by the echo-tracking method. The echo tracking method measures extent of the displacement by tracking the initialized phase pattern of the radio frequency (RF) echo signal. Hokanson et al. [9] have developed an ultrasonic echo-tracking device that allows arterial wall motion to be measured transcutaneously using the standard pulse reflection technique. The motion of the echoes from the arterial wall was tracked by a gated threshold detector and converted into an analog output suitable for recording. The echo tracking method currently used for measuring arterial wall motion has an accuracy of one sixteenth of a wavelength which is an accuracy of 13 μm at every 1 mm/s with a 7.5 MHz probe [10].

Utilizing such an echo tracking method, it is possible to accurately and dynamically detect the displacement of a specific point on the surface of a bone. By detecting the displacement of multiple points on the bone surface under dynamic loading, it may be possible to detect dynamic bone deformation. The final goal of our investigations is to develop a method that can noninvasively detect bone deformation under loading in vivo by ultrasonic echo tracking method. For this purpose, a preliminary study was performed to confirm that our method had sufficient precision to detect bone surface deformation by conducting in vitro three-point bending tests of bone specimens.

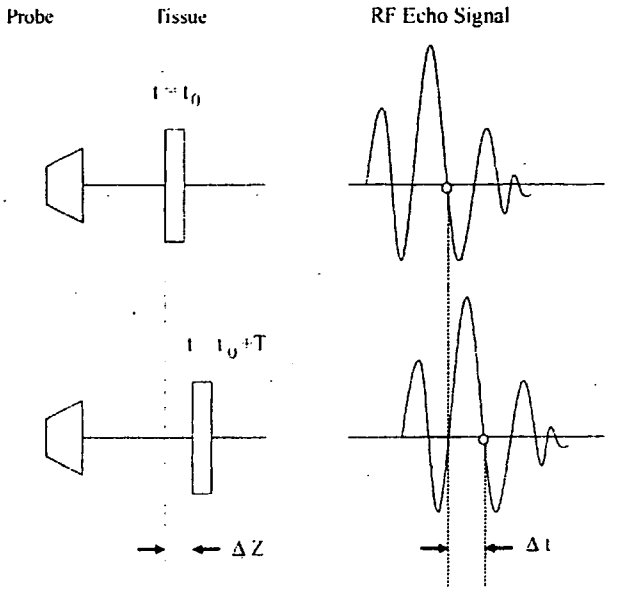

Fig. 1. A diagram of the principal of echo tracking method. Tissue at a certain depth is displaced at time ($t=t_0$) so that it moves away from the probe for a minute distance, ΔZ, during a single cycle of an ultrasonic wave pulse, T. This causes phase delay of a RF echo signal from a tissue for a very short period of time, Δt.

2. Materials and methods

2.1. Echo tracking method

The accuracy of measuring the distance from a probe based on B-mode images depends on the ultrasound wave length and is the order of about 210 μm at a frequency of 7.5 MHz. In contrast, the echo tracking method is a technique measuring minute displacement of a certain point on a tissue with superior accuracy to standard ultrasound by detecting a wave pattern in a RF echo signal reflected from the tissue. For example, it is assumed that a tissue at a certain depth is displaced at time ($t=t_0$), so that it moves away from a probe for a small distance of ΔZ during a single cycle period of an ultrasonic wave pulse, T. This causes phase delay of the RF echo signal from the tissue for a very small period of time, Δt (Fig. 1). The echo tracking method measures extent of the displacement by tracking the initialized phase pattern of the RF echo signal.

We developed the echo tracking system and originally designed the software to utilize the characteristics of the acoustic impedance of bone to accurately measure the displacement on the surface of a bone. A diagram of the echo tracking system specifically designed for bone was shown in Fig. 2. Ultrasound wave was transmitted to the bone surface with a 7.5 MHz linear probe connected to an ultrasonic diagnostic device (SSD-1000, Aloka, Tokyo, Japan). The RF

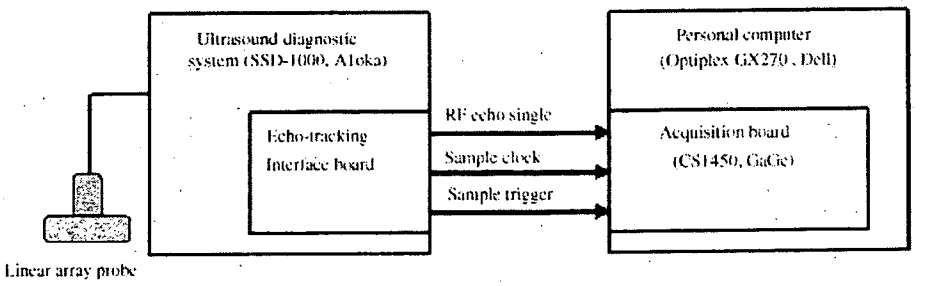

Fig. 2. A block diagram illustrating bone deformation measurement by echo tracking. The RF echo signal is recorded on a personal computer via the echo-tracking interface installed in the ultrasonography device. At the same time, a sample clock signal and sample trigger signal are transmitted to the PC synchronized with a transmit pulse repetition signal.

echo signal reflected from the bone surface was recorded on a personal computer (PC) (Optiplex GX270, Dell, TX, USA) via the echo-tracking interface installed in the ultrasonic diagnostic device. At the same time, a sample clock signal with a frequency of 50 MHz and a sample trigger signal with a frequency of 500 Hz were transmitted to the PC synchronized with a transmitting pulse repetition signal. The analog RF echo signal was converted into a 14-bit digital signal with a sampling frequency of 50 MHz by using a logging board (CS1450, GaGe, Montreal, Canada) installed in the PC and then the data were recorded. The stored RF echo data were interpolated to eight times to allow the detection of phase change with an equivalent sampling frequency of 400 MHz. These interpolated data were processed using software (LabVIEW, National Instruments, TX, USA) and the distance from the probe to each point on the bone surface was calculated.

2.2. *Accuracy assessment of the echo tracking method using an aluminum panel*

With this echo tracking system, we first verified the accuracy of the displacement measured in vitro by an echo tracking system that has been newly developed for measurement of bone deformation. A flat panel of aluminum alloy (65 mm × 85 mm × 10 mm) was fixed to a stepping motor (PK566-A: Oriental motor Co. Ltd., Tokyo, Japan) via a columnar support (TSL120: Nippon Thompson Co. Ltd., Tokyo, Japan) with its surface vertical to the driving axis. To direct ultrasound vertically toward the center of the panel, a 7.5 MHz linear electronic echo probe (UST-5710-7.5: Aloka Co. Ltd., Tokyo, Japan) was fixed to a custom-made probe stand (Aloka Co. Ltd., Tokyo, Japan). The echo probe and the aluminum panel were mounted independently from each other and the distance between them was set at 10 mm in the water bath. The panel was immersed in a plastic water tank (538 mm × 680 mm × 400 mm) and was translated distally along the direction of the echo beam at a displacement rate of 500 μm/s using the stepping motor. The displacement of a central point of the panel surface was measured by the echo tracking system. The displacement of the panel was also measured simultaneously by a linear potentiometer (AT-104: Keyence Corporation, Osaka, Japan) with a proven accuracy of 1 μm at the flat surface of the columnar support above the water (Fig. 3A and B). The accuracy of the echo tracking system was evaluated by comparing these two measurements and the standard deviation (S.D.) of the difference between the displacement measured by the echo tracking and by the potentiometer was calculated. The data-sampling rate for the echo tracking system was 500 Hz and that for the potentiometer was 100 Hz. Throughout the experiment, the water temperature was kept at 24 °C.

2.3. *A three point bending test using a porcine tibia with both ends fully constrained*

To evaluate how accurately the echo tracking system detect bone deformation under loading by monitoring displacement

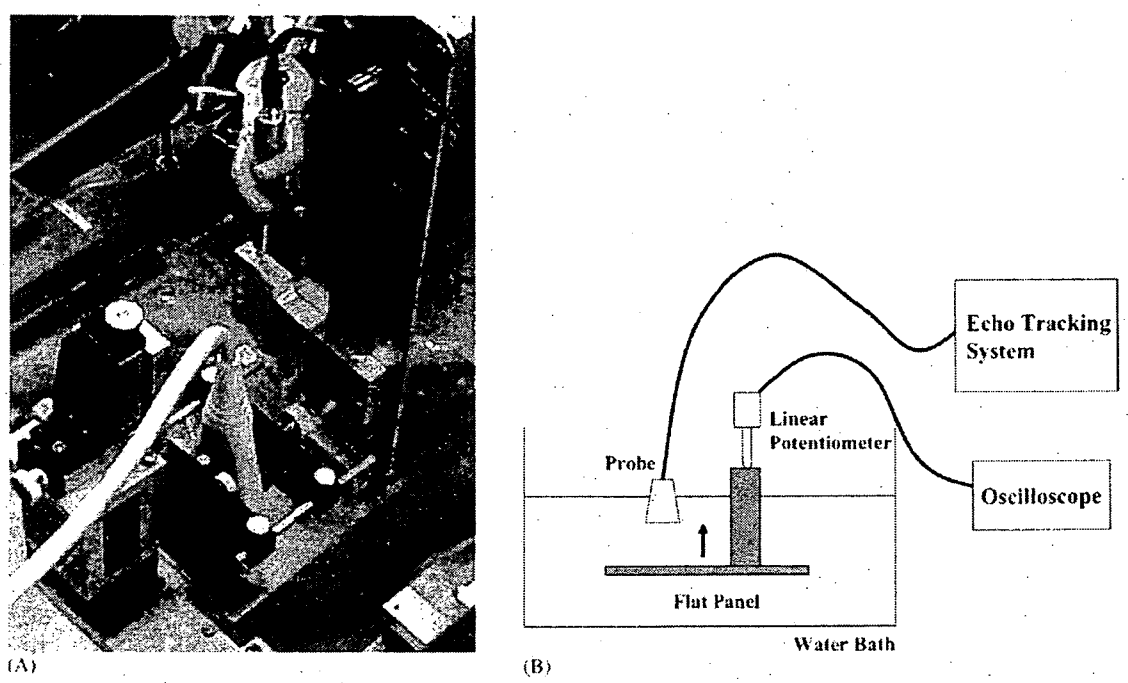

Fig. 3. (A and B) A flat panel fixed to a stepping motor via a columnar support in a plastic water tank vertically moved towards a 7.5 MHz linear electronic echo probe at a displacement rate of 500 μm/s. The displacement of a central point on the panel surface was measured by the echo-tracking system. The displacement of the panel was also measured simultaneously by a linear potentiometer.

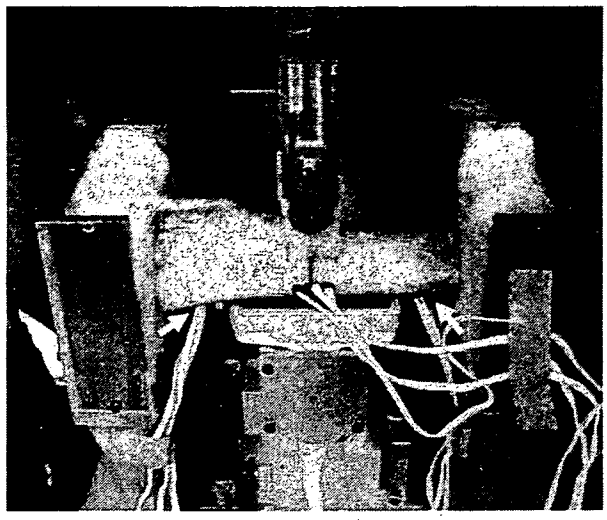

Fig. 4. After removing the soft tissues, the tibia was placed with its medial aspect upwards and both ends of the tibia were fully constrained with dental resin with a span of 214 mm. Two strain gauges were attached to the posterior aspect of the tibia at 50 mm proximal and 50 mm distal from the center of the tibia respectively. Displacement of the osseous surface was measured with the 7.5 MHz linear probe throughout the loading process and strain at each of the gauge sites was simultaneously measured. A single-cycle load and a three-cycle load were applied. (The white arrow on the left indicates the location of proximal strain gauge attached to the posterior bone surface and the white arrow on the right indicates the distal strain gauge.)

of the point on the bone surface, a three-point bending test using a porcine tibia was also performed to measure displacement at the surface of the tibia with the same echo tracking system. An adult porcine tibia with a length of 260 mm (preserved freshly frozen) was used for this experiment. After removing the soft tissues, the tibia was placed horizontally on a testing machine (Tensilon UTM-2.5T: A&D Co. Ltd., Tokyo, Japan) with its medial aspect upwards and both ends of the bone were fully constrained by dental resin (GC Ostron2®: GC, Tokyo, Japan) with a span of 214 mm. Two rosette strain gauges (KGF-1: Kyowa Electronic Instruments, Tokyo, Japan) were attached to the posterior aspect of the tibia at 50 mm proximal and 50 mm distal from the center of the bone respectively. The displacement at the center of the bone surface was measured with the same probe throughout the loading process and the maximum principal strain at each of the gauge sites was measured simultaneously. A single-cycle load and a three cycle-load from 0 to 5780 N were applied at the center of the span of 214 mm in the lateral-medial plane using a resin pusher with a thickness of 25 mm and an actuator speed of 0.1 mm/s over a distance of 0.7 mm (Fig. 4). The sampling rate for the echo tracking system was 500 Hz and that for the strain gauges was 100 Hz. The room temperature was kept at 22 °C and the tibia was kept moistened with physiological saline throughout the experiment. The maximum principal strain measured by the two strain gauges was compared with the displacement shown by the echo tracking system.

2.4. A multi-echo tracking system

We also developed another echo tracking system (multi-echo tracking system) that was capable of simultaneously tracking multiple points. Five points were set along the long axis of the probe at intervals of 10 mm. Displacement at each of the five points was measured simultaneously, and surface deformation of the bone was shown as a third order spline complement curve defined by the displacement at the five points measured by the echo tracking system. The echo tracking system strain (ETS) was calculated by the following equation as a parameter of surface deformation.

$$\mathrm{ETS} = D/L \quad (1)$$

where L is the distance from the first tracking point to the fifth point, and D is the maximum distance from the spline curve to a straight line connecting the first and fifth tracking points. With this multi-echo tracking system, it is assumed that the displacement caused by translation to the direction of the echo beam and rotation in the plane including a loading point and five tracked points, is cancelled.

2.5. A three point bending test with proximal and distal metaphyses supported

To prove the multi-echo tracking system could detect bone deformation even when the measured object underwent some translation, we also measured the deformation of a porcine tibia. After the soft tissues were removed, the tibia with a length of 230 mm was placed horizontally on the testing machine (Servo Pulser, Shimadzu Corporation, Tokyo, Japan) with its medial aspect upwards and both sides of the metaphyses were supported by rollers with a span of 115 mm. A three-point bending load was applied by a resin pusher with a width of 25 mm at the mid point between the two supporting rollers (Fig. 5). Deformation and strain on the posterior surface of the tibia were measured simultaneously with a 7.5 MHz linear probe and two strain gauges (KGF-1, Kyowa, Tokyo, Japan). Five tracking points were set along the long axis of the tibia with the third point corresponding to the site of loading. The echo probe was fixed parallel to the posterior surface of the tibia at a distance of 20 mm. Two strain gauges were attached along the tracking line (a straight line formed by the five tracking points) at 5 mm distal and 5 mm proximal to the third point (center point) and with each gauge axis parallel to the tracking line. The gauge surfaces were waterproofed by coating tar (The Yokohama Rubber Company, Tokyo, Japan). Incremental load increases were applied from a preload of 100 N up to 1500 N. The loading rate was set at 25 N/s. Under each load, the ETS value and the readings of the two strain gauges set parallel to the tracking line were determined. The data sampling rate for echo tracking was 100 Hz and that for the strain gauges was 100 Hz. The correlation between the ETS value and each of the strain gauge readings was calculated with Pearson's cor-

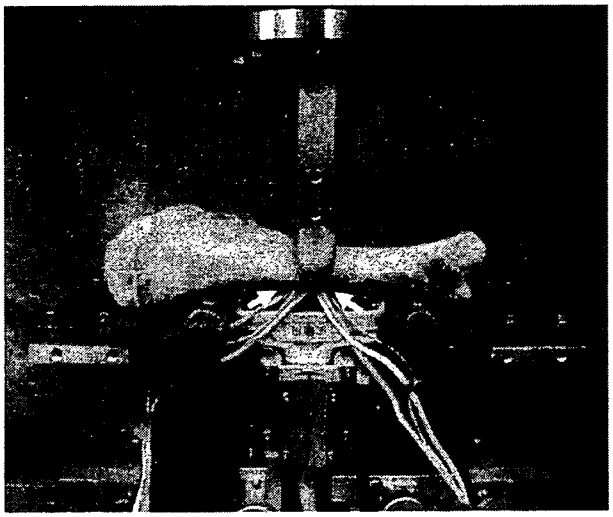

Fig. 5. The extracted porcine tibia was placed horizontally on the testing machine with a medial aspect upwards and both sides of the metaphysis were supported by rollers. Three-point bending loads were applied by a resin pusher from a preload of 100 N up to 1500 N. Deformation and strain of the posterior surface of the tibia were simultaneously measured with a 7.5 MHz linear probe and two strain gauges. Two strain gauges were attached to the tracking line at 5 mm distal and 5 mm proximal to the third tracking point with each gauge axis parallel to the tracking line. The gauge surfaces were waterproofed by coating tar. (The white arrow on the left indicates the location of proximal strain gauge attached to the posterior bone surface and the white arrow on the right indicates the distal strain gauge.)

relation analysis. The room temperature was kept at 22 °C and the tibia was kept moistened with physiological saline throughout the experiment. The sound speed used for the echo tracking measurement was set from the temperature of water in a bath and a bag attached to the probe according to the equation for the relation between water temperature and sound speed proposed by Greenspan [11].

3. Results

For measurement of the displacement of the flat panel, there was excellent linearity between the data obtained by the echo tracking system and the linear potentiometer ($r = 0.999$). The standard deviation (S.D.) of the difference between the displacement measured by the echo tracking system and that measured by the potentiometer was ±2.6 μm.

In the three-point bending test of the porcine tibia, the maximum principal strain recorded by the strain gauge set at 50 mm proximal to the loading point under a load of 5780 N (the maximum load) was 1077 micro strain and that at 50 mm distal was 1350 micro strain, whereas the displacement measured by echo tracking was 678.5 μm. The strain gauge readings and those of the echo tracking system showed excellent linearity with a correlation coefficient of 0.999 for the proximal strain gauge and 0.996 for the distal gauge (Fig. 6). The curve relating the load magnitude with the data obtained from each strain gauge was a typical hysteresis loop, indicating the measured bone was a visco elastic material. The curve for the relationship between the load magnitude and the displacement of the echo tracking system was also a hysteresis loop (Fig. 7).

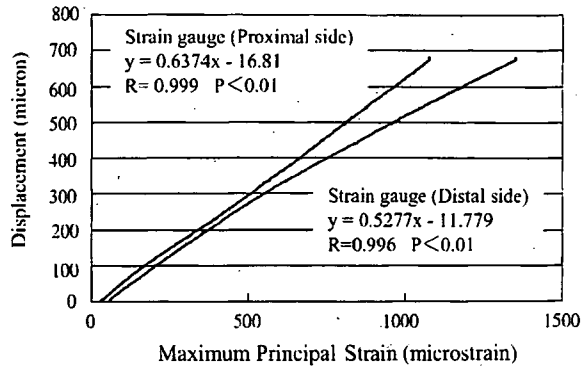

Fig. 6. Result of the single-cycle load in the three-point bending test of the porcine tibia. The graph showed that the strain gauge readings and those with the echo tracking system had an excellent linearity with a correlation coefficient of 0.999 and 0.996 all through the loading cycles.

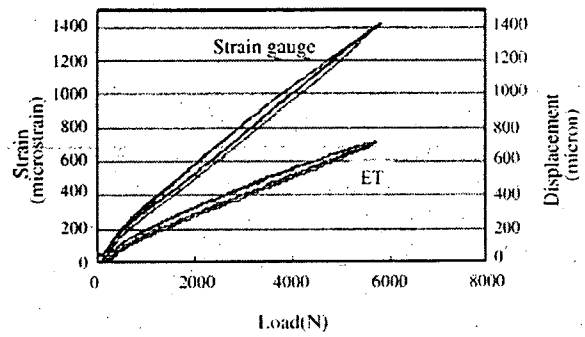

Fig. 7. Result of the three-cycle load in the three-point bending test of the porcine tibia. The curve relating the load magnitude with the data obtained from the strain gauge of the distal side was a typical hysteresis loop, indicating that the measured object was a viscoelastic material. The curve for the relationship between the load magnitude and the displacement of the echo tracking system was also a hysteresis loop.

In the study with the multi-echo tracking system, the strain readings of each gauge and the data from the entire system showed a perfect linear increase with the load. There was a linear relation between echo tracking data and each of the strain gauges ($r = 0.998$ and 0.998, respectively) (Fig. 8A and B). The reading for the gauge axis parallel to the tracking line and the maximum principal strain on the distal gauge at 1500 N was 1154.6 and 1160.4 micro strain, respectively. The angle of the direction of the maximum principal strain was 7° with reference to the echo tracking line.

4. Discussion

Bone shows deformation in response to an applied load. By quantitatively measuring this deformation, it is possible to assess the mechanical properties of bone material. Because

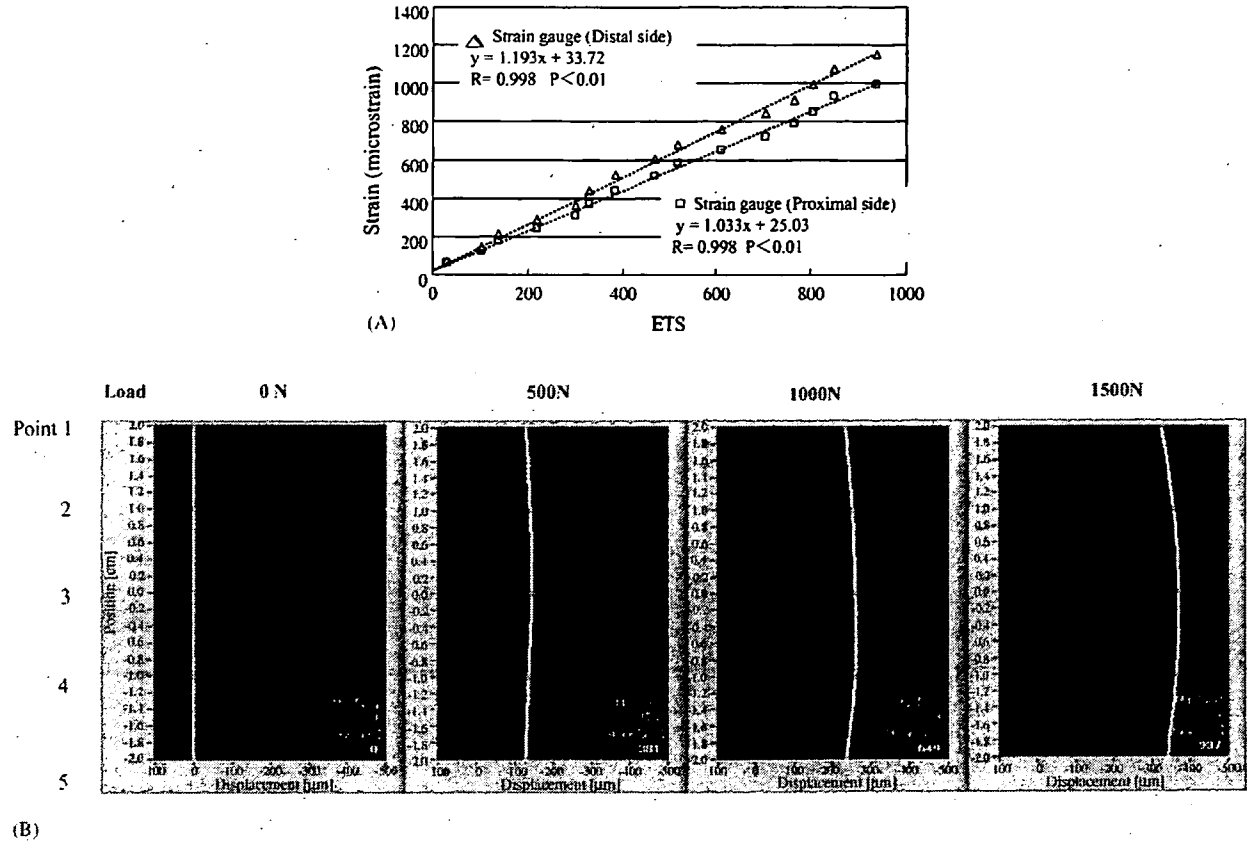

Fig. 8. (A) Result of the three-point bending test of the porcine tibia with the multi-echo tracking system. The strain readings of each gauge and the data from the entire system showed a perfect linear increase with the load. There was a linear relation between echo tracking data and each of the strain gauges ($r = 0.998$ and 0.998, respectively). (B) Result of the displacements at the five tracked points under the loads of 0, 500, 1000 and 1500 N. The surface deformation was visualized by a third order spline complement curve. The surface deformation increased with the increase of the load.

bone is a viscoelastic material, we can estimate its strength by measuring the elasticity, viscosity, and plasticity under dynamic loading. In this study, we attempted to develop an echo tracking method to noninvasively detect bone deformation under a load.

Numerous quantitative measurement methods using ultrasound have been tested to evaluate the elastic properties of bone or the fracture risk [12]. The axial transmission technique was based on the propagation of guided ultrasound waves along the bone surface. A set of ultrasound transducers (transmitters and receivers) was placed on the skin along the bone to measure the velocity of ultrasound waves passing through the cortical layer of the bone parallel to its axis. Sievanen et al. [13] reported in their study of the axial transmission technique that the cortical density was the only determinant of speed of sound measured in the radial and tibial shafts in vivo. The technique of measuring broadband ultrasound attenuation (BUA) and sound of speed (SOS) for the calcaneus was recently developed. Ultrasound transmitted to the calcaneus penetrates the bone and is detected by the receiver located on the opposite side. Then the stiffness of the bone is calculated from the measured BUA and SOS values. This stiffness index is reported to be closely correlated with the regional bone mineral density measured by dual energy X-ray absorptiometry (DXA) [14]. These methods of quantitative evaluation by ultrasound technology have been based on measurement of the speed, permeability, and attenuation of ultrasound transmitted through the bone. In this respect, the echo tracking method that measures bone deformation differs markedly from these preceding ultrasound techniques.

Ultrasonography can clearly visualize the bone surface because the acoustic impedance of osseous tissue differs greatly from that of the surrounding soft tissues. However, the spatial resolution of B-mode images is not better than 100 μm. Therefore, measurement of bone deformation from B mode images is thought to lack sufficient precision, because resolution of better than 10 μm is considered to be necessary to detect deformation compatible to that measured by a strain gauge, which can detect deformation of 0.001 μm when the gauge length is 1 mm (the smallest available gauge). Thus, much more accurate measurement technology has been needed. Measurement of bone surface displacement using the echo tracking fulfils this requirement. The echo tracking method currently used for measuring arterial wall motion has an accuracy of one-sixteenth of a wave length, which is an accuracy of 13 μm at every 1 mm/s with a 7.5 Hz probe. The

system was further improved to measure minute displacement of the bone and a much better precision of 2.6 μm could be obtained by improving the software to utilize the characteristics of the acoustic impedance of bone, so that minute displacement of tracked points on the bone surface could be measured.

The purpose of the first three-point bending test in which both ends were fully constrained was to evaluate whether the echo tracking system could in fact detect bone deformation accurately because the surface of bone was not flat and there was a possibility of the surface morphology changing when deformed. The accuracy of the system was assessed by directly comparing the data from our echo tracking method with those simultaneously recorded by the strain gauges. In this experiment, bone deformation should be regulated to occur in the direction of the echo beam. Because the probe was mounted firmly by an external support and faced the direction of loading, the echo tracking system could only detect displacement in the beam direction. The system used in this experiment could only detect displacement of a single point, so translation of the measured object should have been avoided. From the result of the experiment, we could prove that the correlation between the strain-related data from the echo tracking and the strain gauge readings was excellent. Therefore, the echo tracking method provided sufficient accuracy for detection of bone surface deformation.

Under a cyclic load, the system was able to monitor bone viscoelasticity because the load versus displacement curve was a hysteresis loop. It is well known that bone shows vicsoelasticity, but its nature has not been sufficiently investigated in vivo, because few techniques have been available to assess bone viscoelasticity in vivo. Only Moorcroft et al. [15] and Ohnishi et al. [16] have already investigated viscoelasticity in vivo using an external fixation system. To date, no method has been available to noninvasively assess the viscoelasticity of bone in vivo. However, it is very useful to assess bone viscoelasticity because it varies markedly during the process of fracture healing. The hysteresis loop shown by the echo tracking method indicated that it could be used to quantitatively assess in vivo viscoelasticity noninvasively in the future. Further investigations using bone models of known viscoelasticity will be needed to confirm the precision of the echo tracking system.

The purpose of the second three-point bending test in which both sides of the metaphyses were supported by rollers was to prove that the echo tracking system could detect bone deformation even when the measured object underwent some translation. Measurement of only one point is inadequate for detecting deformation because the displacement caused by translation of a moving object will be mixed. Accordingly, measurement of multiple points should be necessary to cancel the displacement caused by translation. Using the system with the multiple tracked points set along the straight line, it is assumed that the displacement caused by translation to the direction of the echo beam and rotation in the plane including the loading point and the five tracked points is cancelled. The test in which both metaphyses were simply supported by rollers allows the tibia to translate to the direction of loading and to rotate within the frontal plane (the plane that includes the loading point and both supporting points). The magnitude of the strain measured by the strain gauges was an average strain of 1 mm gauge length, while the ETS measured an average strain of 40 mm. However, the linearity of both methods was very strong, indicating that only deformation components from the displacement data of five tracked points could be extracted even when the measured object underwent some translation. The strain along the tracking line was very close to the maximum principal strain and the difference in the direction of both was very small (only 7°). This indicated that the direction of strain at the center of the posterior surface of the tibia generated by three-point bending was almost parallel to that of the echo tracking line. By echo tracking measurement of multiple points, it is possible to optimize the detection environment depending on the pattern or mode of bone deformation under specific mechanical conditions by changing the interval and number of the measured points.

Our method has the technical limitation of only detecting deformation in the plane that includes the measured points because the tracking points were all located on a straight line. When bone deformation occurs in multiple planes, only the component of deformation in the measured plane can be detected, and the other components cannot be measured with the current system. To overcome this limitation, a measurement system should be developed with a three-dimensional distribution of multiple tracking points that is capable of detecting multi-directional deformation.

Our echo tracking system had sufficient accuracy to detect bone surface deformation and could monitor the viscoelasticity of bone. Although further investigations will be necessary before this method can be applied to in vivo measurement, our echo tracking method might have a considerable potential for noninvasive measurement of the viscoelasticity and plasticity of bone.

Acknowledgement

This work was funded in part by the grant from the Pharmaceutical and Medical Devices Agency of Japan.

References

[1] Hung CT, Allen FD, Pollack SR, Brighton CT. Intracellular Ca^{2+} stores and extracellular Ca^{2+} are required in the real-time Ca^{2+} response of bone cells experiencing fluid flow. J Biomech 1996;29(11):1411–7.

[2] Johnson DL, McAllister TN, Frangos JA. Frangos JA. Fluid flow stimulates rapid and continuous release of nitric oxide in osteoblasts. Am J Phys 1996;271(1Pt1):E205–8.

[3] Reich KM, Frangos JA. Effect of flow on prostaglandin E2 and inositol trisphosphate levels in osteoblasts. Am J Phys 1991;261(3Pt1): C428–32.